

1 Analysis of particulate emissions from tropical biomass 2 burning using a global aerosol model and long-term 3 surface observations

4 C.L.Reddington¹, D.V. Spracklen¹, P. Artaxo², D.A. Ridley^{1,3}, L.V. Rizzo⁴ and A.
5 Arana²

6 [1] {School of Earth and Environment, University of Leeds, Leeds, United Kingdom}

7 [2] {Department of Applied Physics, Institute of Physics, University of Sao Paulo, Sao Paulo,
8 Brazil}

9 [3] {now at Department of Civil and Environmental Engineering, Massachusetts Institute of
10 Technology, USA}

11 [4] {Institute of Environmental, Chemical and Pharmaceutical Sciences, Federal University of
12 Sao Paulo, Diadema, Brazil}

13 Correspondence to: C. L. Reddington (c.l.s.reddington@leeds.ac.uk)

15 Abstract

16 We use the GLOMAP global aerosol model evaluated against observations of surface
17 particulate matter (PM_{2.5}) and aerosol optical depth (AOD) to better understand the impacts
18 of biomass burning on tropical aerosol over the period 2003 to 2011. Previous studies report a
19 large underestimation of AOD over regions impacted by tropical biomass burning, increasing
20 particulate emissions from fire by up to a factor 6. To explore the uncertainty in emissions we
21 use three satellite-derived fire emission datasets (GFED3, GFAS1 and FINN1) in the model,
22 in which tropical fires account for 66-84% of global particulate emissions from fire. The
23 model underestimates dry season PM_{2.5} concentrations in regions of high fire activity in
24 South America and underestimates AOD over South America, Africa and Southeast Asia.
25 Underestimation of AOD over tropical regions impacted by biomass burning is slightly
26 reduced, relative to previous studies. Where coincident observations of surface PM_{2.5} and
27 AOD are available we find a greater model underestimation of AOD than PM_{2.5} at some
28 sites. Increasing particulate emissions to improve simulation of AOD can therefore lead to
29 overestimation of surface PM_{2.5} concentrations. With FINN1 emissions increased by a factor
30 of 1.5 the model reasonably simulates PM_{2.5} concentrations and AOD in South America and

1 AOD over Southeast Asia, but underestimates AOD over Africa. The model with GFAS1
2 emissions better matches observed PM2.5 and AOD when emissions are increased by a factor
3 of 3.4, with the exception of Equatorial Asia where a scaling factor of 1.5 is adequate. The
4 model with GFED3 emissions increased by a factor of 1.5 reasonably simulates PM2.5
5 concentrations and AOD in active deforestation regions in South America and AOD in
6 Equatorial Asia, but requires a larger scaling factor to capture observed AOD in Africa,
7 Indochina and elsewhere in South America. The model with GFED3 emissions poorly
8 simulates observed seasonal variability of surface PM2.5 and AOD in regions where small
9 fires dominate, providing independent evidence that GFED3 omits emissions from small fires.
10 Seasonal variability of both PM2.5 and AOD in South America is better simulated by the
11 model using FINN1 and GFAS1 emissions. Detailed observations of the vertical profile of
12 aerosol over biomass burning regions are required to better constrain emissions and modelled
13 AOD.

14

15 **1. Introduction**

16 Open biomass burning is an important source of trace gases and particulate matter (PM) to the
17 atmosphere (Crutzen and Andreae, 1990; Andreae and Merlet, 2001; Van der Werf et al.,
18 2010). Biomass burning emissions can influence weather (Kolusu et al., 2015; Gonçalves et
19 al., 2015; Tosca et al., 2015) and climate (Ramanathan et al., 2001; Tosca et al., 2013;
20 Jacobson, 2014) directly, by scattering and absorbing solar radiation (Johnson et al., 2008;
21 Sakaeda et al., 2011), and indirectly, by modifying cloud properties (Andreae et al., 2004;
22 Feingold et al., 2005; Tosca et al., 2014). The influence of biomass burning aerosol on surface
23 radiation can have subsequent impacts on the biosphere. For example, smoke plumes from
24 biomass burning have been observed to increase plant productivity, through increasing the
25 amount of diffuse radiation (Oliveira et al., 2007; Doughty et al., 2010), which has been
26 shown to be a regionally important process over the Amazon (Rap et al., 2015). PM from
27 biomass burning can substantially degrade regional air quality leading to adverse effects on
28 human health (Emmanuel, 2000; Frankenberg et al., 2005; Johnston et al., 2012; Jacobson,
29 2014; Reddington et al., 2015). A better understanding of particulate emissions is needed to
30 improve predictions of the impacts on biomass burning on climate and air quality. Here we
31 use a global aerosol model with tropical observations of surface PM and aerosol optical depth
32 (AOD) to better understand the impact of tropical fires on atmospheric aerosol.

1 The spatial and temporal distribution of fires depends on climate, vegetation and human
2 activities. At the global scale, fire emissions are dominated by burning in the tropics (van der
3 Werf et al., 2010). Anthropogenic activity can increase the occurrence of fires either directly,
4 through deforestation fires and agricultural residue burning (van der Werf et al., 2010), or
5 indirectly, through land-use/land-cover change that acts to increase the fire susceptibility of
6 the land surface e.g. forest fragmentation in the Amazon (Cochrane and Laurance, 2002) and
7 large-scale drainage of peatlands in Indonesia (Field et al., 2009; Carlson et al., 2012). Human
8 activity can also reduce the occurrence of fires, directly through fire suppression and
9 indirectly through reducing and fragmenting fuel loads which limits fire spread (Bistinas et
10 al., 2014). Over the 21st century, predicted changes in rainfall and temperature may increase
11 forest water stress and subsequent fire occurrence in tropical forests (Cox et al., 2008;
12 Golding and Betts, 2008; Malhi et al., 2009). The incidence of fire and resulting emissions are
13 therefore sensitive both to changing climate and changes in land-use (Heald and Spracklen,
14 2015).

15 High temporal and spatial variability in biomass burning emissions coupled with the
16 difficulties involved in conducting measurements in remote tropical regions lead to major
17 challenges for their quantification. In recent years, global estimates of biomass burning
18 emission fluxes have mostly been obtained using satellite remote sensing (e.g., van der Werf
19 et al., 2006, 2010; Reid et al., 2009; Wiedinmyer et al., 2011; Kaiser et al., 2012; Zhang et al.,
20 2012; Ichoku and Ellison, 2014), which provides long-term observations with relatively high
21 spatial coverage. A range of satellite products and methods are utilised to derive fluxes of
22 aerosol and gas-phase species emitted from fires. The most common methods use satellite-
23 retrieved burned area, active fire counts, and/or fire radiative power (FRP) in combination
24 with biogeochemical models (when using burned area) and/or species-specific emission
25 factors obtained from laboratory experiments and field observations (e.g., Hoelzemann et al.,
26 2004; Ito and Penner, 2004; 2005; van der Werf et al., 2006, 2010; Wiedinmyer et al., 2006;
27 2011; Schultz et al., 2008; Kaiser et al., 2012). Large uncertainties are associated with
28 satellite observations of fires and with the various methods used to calculate emissions fluxes
29 from the observational data (e.g. Ito and Penner, 2005; Reid et al., 2009; Konovalov et al.,
30 2014)

31 Previous studies using satellite-derived emissions and atmospheric models to investigate the
32 properties and impacts of biomass burning aerosol have found a persistent underestimation of
33 AOD observed in most tropical biomass burning regions (Matichuk et al., 2007; 2008; Chin et

1 al., 2009; Petrenko et al., 2012; Kaiser et al., 2012; Ward et al., 2012; Tosca et al, 2013). In
2 general, modelling studies have required biomass burning emissions or concentrations of
3 biomass burning aerosol to be increased by factors ranging from ~1.5 to ~6 in order to match
4 satellite and ground based observations of AOD (Matichuk et al., 2007; 2008; Johnson et al.,
5 2008; Sakaeda et al., 2011; Johnston et al., 2012; Kaiser et al., 2012; Tosca et al., 2013;
6 Marlier et al., 2013). The underestimation of AOD observed in biomass burning regions has
7 been attributed to a number of factors (see e.g., Kaiser et al., 2012) including: i)
8 underestimation of biomass burning emission fluxes; ii) errors in modelling the atmospheric
9 distribution and properties of biomass burning aerosol; and iii) uncertainties in the calculation
10 of AOD.

11 Uncertainties associated with the derivation of emission fluxes arise from errors present in the
12 satellite-detection of active fires or burned area (e.g. obscuring of the surface by clouds and
13 smoke, satellite spatial resolution and detection limits, and satellite overpass time), as well as
14 uncertainties in emission factors and fuel consumption estimates. For example, Randerson et
15 al. (2012) suggest that emission datasets based on relatively coarse burned area data
16 (detection limit of ~100 Ha), result in an underestimation of global area burned by ~35%,
17 although this error is not sufficient to fully explain the underestimation of AOD discussed
18 above. Inadequate representation of biomass burning aerosol in models, including errors in
19 the modelled aerosol size distribution, chemical composition, ageing processes, vertical and
20 horizontal transport (including fire emission injection heights) and dry/wet removal from the
21 atmosphere, could also contribute to an underestimation of AOD. The contribution of
22 secondary organic aerosol (SOA) from the oxidation of volatile organic compounds in
23 biomass burning plumes is also a large uncertainty (Jathar et al., 2014; Shrivastava et al.,
24 2015). In the calculation of AOD itself, the uncertainties associated with the assumed optical
25 properties of biomass burning aerosol e.g. their refractive indices, hygroscopicity (uptake of
26 water onto the aerosol), and/or mixing state (i.e. treated as core/shell mixtures,
27 internally/externally mixed etc.) may also contribute to this negative model bias in AOD.

28 Using only AOD to evaluate estimates of biomass burning aerosol emissions can be
29 misleading because AOD depends on many factors in addition to aerosol abundance. Scaling
30 biomass burning emissions to match observed AOD could therefore lead to inaccurate model
31 representation of biomass burning aerosol concentrations and, subsequently, errors in model
32 predictions of the air quality and climate effects of biomass burning aerosol. Although there
33 has been extensive use of AOD retrievals to evaluate model predictions of biomass burning

1 aerosol, thus far there have been relatively few studies to use aerosol measurements to
2 thoroughly evaluate these models (e.g., Liousse et al., 2010; Daskalakis et al., 2015).

3 In this study, we evaluate a global aerosol microphysics model against observations of aerosol
4 mass concentrations in addition to AOD to better understand the discrepancy in modelled
5 biomass burning AOD and to ultimately improve estimates of biomass burning aerosol. We
6 also compare three different biomass burning emission inventories to investigate regional
7 differences between emissions and identify the best fit emissions for future modelling studies.

8

9 **2. Observations**

10 To evaluate the simulated distribution of PM at the surface, we use long-term *in-situ*
11 measurements of PM_{2.5} (particulates with aerodynamic diameters < 2.5 μm) mass
12 concentrations conducted at four ground stations in the Amazon region (Alta Floresta, Porto
13 Velho, Santarem and Manaus). The location and observation period are detailed for each
14 station in Table S1 in the supplementary material. Figure S1 shows the measured PM_{2.5}
15 concentrations at each station between 2003 and 2011, demonstrating the data coverage.

16 The PM_{2.5} measurements were made using gravimetric filter analysis and the measurement
17 duration ranges from less than 1 day to more than 10 days. Particles were sampled under
18 ambient relative humidity (RH) conditions (typically in the range of 80-100% RH). The
19 sampled filters were weighed after 24 hours of equilibration at 50% RH and 20°C. Amazonian
20 submicrometer aerosol particles have growth factors of ~1.1-1.3 at 90% RH (Zhou et al, 2002;
21 Rissler et al., 2006) so we estimate that water represents roughly ~10-20% of the PM_{2.5} mass
22 concentrations at measurement conditions. Uncertainties related to filter handling, sampling
23 and analysis are estimated as 15% of particle mass. Further information on the measurements
24 conducted at the Manaus and Porto Velho stations can be found in Artaxo et al. (2013). Our
25 evaluation of PM_{2.5} is restricted to Amazonia since there are few long-term observations of
26 PM_{2.5} in other tropical regions impacted by biomass burning.

27 The measurement stations at Porto Velho and Alta Floresta are located in the arc of
28 deforestation and are strongly impacted by fresh biomass burning emissions (Fig. 1). The
29 Santarem and Manaus stations are located within forest reservations and are impacted by
30 transported regional biomass burning emissions in the dry season. The Santarem station is
31 located in Para, where the number of fire hotspots observed by satellites during the dry season
32 are typically a factor of ~10 greater than the number observed in Amazonas, where the Manaus

1 station is located. Thus in the dry season, PM_{2.5} concentrations measured at Santarem are
2 typically higher than those measured at Manaus.

3 To evaluate the simulated distribution of AOD, we use observations of spectral columnar
4 AOD measured by the Aerosol Robotic Network (AERONET) using ground-based Cimel sun
5 photometers (Holben et al., 1998). Specifically, we use Level 2.0 (quality assured) daily
6 average AOD retrieved at 440 nm from 27 AERONET stations detailed in Table S1. We
7 selected stations located within regions influenced by tropical biomass burning (Southeast and
8 Equatorial Asia, Central and Southern Africa, and the Amazon region in South America) that
9 have more than one year of relatively continuous data (automatic cloud screening leads to
10 gaps in the dataset) between 2003 and 2011. We note that whilst the majority of cloud-
11 contaminated AOD data is removed; comparisons with co-located Micro-Pulse Lidar Network
12 observations indicate that some contamination from thin cirrus clouds may remain, possibly
13 leading to small positive biases in observed AOD (Huang et al., 2011; Chew et al., 2011).

14 To compare modelled and observed PM_{2.5} and AOD, daily-mean model output was linearly
15 interpolated to the location (latitude, longitude and altitude above sea level) of each ground
16 station. Model data that corresponded to gaps in the observation datasets were removed prior
17 to calculating monthly-mean values used in the analysis. The modelled PM_{2.5} concentration
18 is calculated for dry aerosol, omitting the contribution of water to the total mass, thus
19 modelled PM_{2.5} concentrations may be underestimated compared to the observations, which
20 include some contribution from the mass of water.

21

22 **3. Model description**

23 **3.1 Global aerosol microphysics model**

24 The global distribution of aerosol was simulated using the 3-D Global Model of Aerosol
25 Processes (GLOMAP; Spracklen et al., 2005a,b; Mann et al., 2010), which is an extension to
26 the TOMCAT chemical transport model (Chipperfield, 2006). Simulations were run for the
27 period 2003 to 2011. Large scale atmospheric transport and meteorology in TOMCAT are
28 specified from European Centre for Medium-Range Weather Forecasts (ECMWF) analyses,
29 updated every 6 hours and linearly interpolated onto the model time-step. The model runs at a
30 horizontal resolution of $2.8^{\circ} \times 2.8^{\circ}$ with 31 vertical model levels between the surface and 10
31 hPa. The vertical resolution in the boundary layer ranges from ~60 m near the surface to ~400

1 m at ~2 km above the surface. GLOMAP has been extensively evaluated in previous studies
2 against aerosol observations (Mann et al., 2010, 2014; Spracklen et al., 2011a,b; Browse et
3 al., 2012; Schmidt et al., 2012; Scott et al., 2014; Reddington et al., 2011, 2013, 2014). Below
4 we describe the features of the model relevant for this study, please see Spracklen et al.
5 (2005a) and Mann et al. (2010) for more detailed descriptions of the model.

6 GLOMAP simulates the mass and number of size resolved aerosol particles in the
7 atmosphere, including the influence of aerosol microphysical processes on the particle size
8 distribution. These processes include nucleation, coagulation, condensation, ageing,
9 hygroscopic growth, cloud processing, dry deposition, and nucleation/impact scavenging. The
10 aerosol particle size distribution is represented using a two-moment modal scheme with seven
11 log-normal modes (Mann et al., 2010). Within each mode, aerosol particles are treated as
12 internally mixed. GLOMAP treats the following aerosol species: black carbon (BC),
13 particulate organic matter (POM), sulphate (SO₄), sea spray and mineral dust. Biogenic SOA
14 is formed in the model via the reaction of biogenic monoterpenes with O₃, OH and NO₃,
15 which produces a gas-phase oxidation product that condenses with zero vapour pressure onto
16 pre-existing aerosol (Spracklen et al., 2006, 2008). Concentrations of oxidants are specified
17 using monthly-mean 3-D fields at 6-hourly intervals from a TOMCAT simulation with
18 detailed tropospheric chemistry (Arnold et al., 2005) linearly interpolated onto the model
19 time-step. Monthly mean emissions of biogenic monoterpenes are taken from the Global
20 Emissions Initiative (GEIA) database (Guenther et al., 1995). Size-resolved emissions of
21 mineral dust are prescribed from daily-varying emissions fluxes provided for AEROCOM
22 (Dentener et al., 2006).

23 For this study, anthropogenic emissions of sulphur dioxide (SO₂), BC and organic carbon
24 (OC) were specified using the MACCity emissions inventory (Lamarque et al., 2010; Granier
25 et al., 2011), which provides annually varying emissions for the period 1979-2010. For
26 simulations in the year 2011 we used MACCity anthropogenic emissions from 2010. Biomass
27 burning emissions of SO₂, BC and OC were specified using three different satellite-derived
28 emission datasets, which are described in detail in Section 3.3. We convert OC to POM using
29 a prescribed POM:OC ratio of 1.4, which is at the lower end of the range prescribed in other
30 global models (1.4 to 2.6) (Tsigaridis et al., 2014). The fire emissions were injected into the
31 model over six ecosystem-dependent altitudes between the surface and 6 km recommended by
32 Dentener et al. (2006). In the regions studied in this paper (South America, Africa and
33 Southeast Asia), the fire emission injection heights range between the surface and an altitude

1 of ~3 km asl. The largest fraction of the fire emissions, ranging from ~99% of emissions in
2 Equatorial Asia to 88% in Indochina, are injected below 1 km asl (or at surface level if the
3 altitude of the model level exceeds 1 km asl). Analysis of smoke plume heights has
4 demonstrated that most smoke emissions from fires occur within the boundary layer (Val
5 Martin et al., 2010).

6 Primary carbonaceous aerosol particles are assumed to be non-volatile and are emitted into
7 the model with a fixed log-normal size distribution, assuming a number median diameter of
8 150 nm for biomass burning emissions and 60 nm for fossil fuel emissions and modal width
9 (σ) of 1.59. Several previous studies have investigated the impacts of the uncertainty in the
10 assumed emission size distribution on simulated aerosol and cloud condensation nuclei
11 concentrations (Pierce et al., 2007; Pierce and Adams, 2009; Reddington et al., 2011; 2013;
12 Lee et al., 2013) and aerosol radiative forcing (Bauer et al., 2010; Spracklen et al., 2011b;
13 Carslaw et al., 2013). An assumption of a number median diameter of 150 nm for biomass
14 burning emissions is reasonably consistent with measurements of the size distributions of
15 fresh biomass burning aerosol from grassland (100 – 125 nm) and deforestation (100 – 130
16 nm) fires (Reid et al., 2005 and references therein). Once emitted into the model, the
17 components of primary carbonaceous aerosol (BC and OC) are assumed to mix
18 instantaneously and are initially treated as non-hygroscopic. Once these particles have
19 accumulated 10 monolayers of soluble material (assumed to be SOA and H₂SO₄) through
20 condensation, they are transferred directly to the corresponding soluble Aitken or
21 accumulation mode to account for ageing. For a discussion of the treatment of organic aerosol
22 within global aerosol models see Tsigaridis et al. (2014).

23 **3.2 Calculation of aerosol optical depth**

24 AOD was calculated from the simulated aerosol size distribution using Mie theory assuming
25 spherical particles (Grainger et al., 2004) that are externally mixed within each log-normal
26 mode. For this study, modelled AOD was calculated at a wavelength of 440 nm using
27 component-specific refractive indices at the closest wavelength available (468 nm) from
28 Bellouin et al. (2011). Water uptake plays a significant role in determining AOD, altering the
29 refractive index and the size distribution of the aerosol. The water uptake for each soluble
30 aerosol component is calculated on-line in the model according to Zdanovskii-Stokes-
31 Robinson (ZSR) theory, which estimates the liquid water content as a function of solute
32 molarity (Stokes and Robinson, 1966). We assign moderate hygroscopicity to POM in the

1 soluble modes, consistent with a water uptake per mole at 65% of SO₄ (Mann et al., 2010).
2 The resulting daily-mean wet radii and refractive indices are used to calculate the daily-mean
3 aerosol extinction. Using hourly-mean values of water uptake increased simulated daily AOD
4 on average by less than 1%.

5 **3.3 Biomass burning emissions**

6 In this study we compare three different satellite-derived datasets of biomass burning
7 emissions: the Global Fire Emissions Database version 3 (GFED3; van der Werf et al., 2010),
8 the National Centre for Atmospheric Research Fire Inventory version 1.0 (FINN1;
9 Wiedinmyer et al., 2011) and the Global Fire Assimilation System version 1.0 (GFAS1;
10 Kaiser et al., 2012). The key aspects of these emission inventories are summarised in Table 1.
11 We complete GLOMAP simulations for the period 2003 to 2011 where all three emission
12 datasets are available.

13 GFED3 provides monthly-mean fire emissions of aerosol and gas-phase species from 1997 to
14 2011 at 0.5°×0.5° resolution (van der Werf et al., 2010). GFED3 emissions are derived using
15 the monthly-mean time series of global burned area estimates from Giglio et al. (2010). For
16 1997-2000, the fire emissions are based on burned area derived from the TRMM Visible and
17 Infrared Scanner (VIRS) and Along-Track Scanning Radiometer (ATSR) active fire data and
18 estimates of plant productivity derived from observations from the Advanced Very High
19 Resolution Radiometer (AVHRR). For November 2000 onwards, the fire emissions are based
20 on estimates of burned area, active fire detections, and plant productivity from the MODerate
21 resolution Imaging Spectroradiometer (MODIS) instrument on-board the Terra and Aqua
22 satellites. To derive total carbon emissions the satellite datasets are combined with estimates
23 of fuel loads and combustion completeness for each monthly time step from the Carnegie-
24 Ames-Stanford-Approach biogeochemical model. The carbon emission fluxes are converted
25 to trace gas and aerosol emissions using species specific emission factors compiled by
26 Andreae and Merlet (2001). From 2003 onwards, GFED3 fire emissions are available on a
27 daily time step, developed using detections of active fires from MODIS (Mu et al., 2011).
28 Daily GFED3 fire emissions were implemented in GLOMAP for the period 2003-2011.

29 FINN1 provides daily fire emissions of aerosol and gas-phase species from 2002 to 2012 on a
30 1 km² grid (Wiedinmyer et al., 2011). FINN1 fire emissions are based on detections of active
31 fires (specifically their location and timing) from the MODIS Fire and Thermal Anomalies
32 Product (Giglio et al., 2003). FINN1 also uses the MODIS Land Cover Type product to

1 specify land cover classes and the MODIS Vegetation Continuous Fields product to identify
2 the fractions of tree and non-tree vegetation, and bare ground. Specifically, the emitted mass
3 (E) of a certain species (i) is calculated using the following equation (Seiler and Crutzen,
4 1980):

$$5 \quad E_i = A(x, t) \times B(x) \times FB \times ef_i \quad (1)$$

6 Where A is the area burned at time t and location x , B is the biomass loading at location x , FB
7 is the fraction of that biomass that is burned and ef is the emission factor of species i . For each
8 fire count the area burned, A , is assumed to be 0.75 km^2 for fires detected on grassland and
9 savannah land cover classes, and 1 km^2 for those detected on all other land cover classes
10 following Wiedinmyer et al. (2006) and Al-Saadi et al. (2008). Adjustments are made to the
11 assumed burned area if the fire pixel extends partially over bare ground (reducing the burned
12 area by the percentage of bare area assigned to that pixel). Estimates of biomass loading, B ,
13 are taken from Hoelzemann et al. (2004) and are assumed to be land cover specific. The
14 fraction of biomass assumed to burn, FB , in each fire pixel is determined as a function of tree
15 cover using relationships from Ito and Penner (2004) (see Wiedinmyer et al., 2006). Emission
16 factors, ef , for each species are taken from Akagi et al. (2011).

17 GFAS1 provides daily fire emissions of aerosol and gas-phase species from March 2000 to
18 2013 at $0.5^\circ \times 0.5^\circ$ resolution (Kaiser et al., 2012). Like FINN1, GFAS1 uses the observed
19 geo-location of active fires from the MODIS instrument. However, GFAS1 also makes use of
20 the NASA fire products (MOD14 and MYD14) that provide quantitative information on the
21 radiative power of detected fires (Justice et al., 2002; Giglio, 2005). The FRP fields are
22 corrected for observation gaps due to partial cloud-cover by assuming the same FRP areal
23 density throughout the grid cell. Data assimilation is used to further fill observation gaps
24 using information from earlier FRP observations (see Kaiser et al., 2012). Spurious signals
25 from volcanoes, gas flares and other industrial activity are removed from the data. The FRP is
26 converted to the combustion rate of dry matter using land-cover-specific conversion factors
27 based on data from GFED3 (Heil et al., 2010; Kaiser et al., 2012). As for GFED3, species
28 emission rates are calculated using updated emission factors based on Andreae and Merlet
29 (2001).

30 Table 1 gives the total annual amounts of BC and OC aerosol emitted from fires over the
31 tropics for each emission inventory. The total BC and OC emitted from fires in the tropics
32 make up 77-84% and 66-77%, respectively of the global total emissions. FINN1 has the

1 greatest tropical OC emission, with emissions being 47% greater than in GFAS1 and 30%
2 greater than GFED3. Emission of BC is more consistent, with FINN1 BC emissions being
3 13% greater than GFAS1 and 1% greater than GFED3. This results in different OC:BC
4 emission ratios between the datasets with the mean ratio across the tropics varying from 10.0
5 in FINN1, 7.9 in GFED3 and 7.1 in GFAS1.

6 Figure 1a-c shows the spatial distribution of annual total biomass burning emissions of OC
7 from each fire inventory averaged over the period of 2003 to 2011. There are similarities in
8 the general spatial distributions of fire emissions, with all three inventories showing
9 maximum emissions over the tropical savannah and humid subtropical regions of Africa, the
10 arc of deforestation in Amazonia, coastal regions of Indonesia (Sumatra and Kalimantan),
11 northern Australia, and parts of Indochina (particularly Cambodia, Laos and Myanmar).
12 However, Figs. 1d-f show that there are strong regional differences between the different
13 emission inventories. Differences between FINN1 and GFAS1 (Fig. 1e) and FINN1 and
14 GFED3 (Fig. 1f) are more spatially organised than differences between GFAS1 and GFED3
15 (Fig. 1d), which are more spatially heterogeneous.

16 Over Africa, GFED3 gives higher OC emissions in northern tropical savannah and southern
17 humid subtropical regions, with GFAS1 and FINN1 giving higher emissions than GFED3 at
18 the boundaries of these regions and over central Africa. Over Australia, GFED3 gives the
19 highest OC emissions estimates over the tropical savannah region of northern Australia, with
20 GFAS1 giving the highest emissions in the dryer grassland and desert regions further south.

21 Over South America the picture is more complex. In general, FINN1 and GFAS1 emission
22 estimates are higher in northern and eastern Brazil than GFED3, with GFAS1 giving the
23 highest emissions over eastern areas and FINN1 over northern Brazil. FINN1 emissions are
24 generally higher than GFAS1 and GFED3 over the central and southern Amazon region
25 (particularly over the state of Mato Grosso), Peru and generally over northern South America.
26 GFED3 emissions are higher than FINN1 and GFAS1 in northern parts of Bolivia and the
27 northern part of the state of Rondônia in the arc of deforestation.

28 Over South Asia, Indochina and Equatorial Asia, FINN1 gives higher emissions than both
29 GFED3 and GFAS, particularly over Bangladesh, Myanmar and Laos, with the exception of
30 the coastal peatland regions of Sumatra and Kalimantan where GFAS1 and GFED3 give
31 higher emissions than FINN1. The differences in emissions over Indonesia may be explained

1 by a potentially improved representation of tropical peat fire emissions in GFED3 and GFAS1
2 relative to FINN1 (Andela et al., 2013).

3

4 **4. Results**

5 **4.1 Overview of all comparisons**

6 **4.1.1 Particulate matter concentrations in the Amazon region**

7 Figure 2 shows simulated versus observed multi-annual monthly mean PM2.5 concentrations
8 at each of the four ground stations in the Amazon region (see Fig. 1 for site locations). To
9 quantify the agreement between model and observations, we use the Pearson correlation
10 coefficient (r) and normalised mean bias factor (NMBF) as defined by Yu et al. (2006):

$$NMBF = \frac{(\sum M_i - \sum O_i)}{|\sum M_i - \sum O_i|} \left[\exp \left(\left| \ln \frac{\sum M_i}{\sum O_i} \right| \right) - 1 \right]$$

11 where M and O represent the multi-annual monthly mean model and observed values,
12 respectively, for each month i . A positive NMBF indicates the model overestimates the
13 observations by a factor of NMBF+1. A negative NMBF indicates the model underestimates
14 the observations by a factor of 1-NMBF.

15 Figure 2 demonstrates the important contribution of biomass burning to PM2.5 concentrations
16 across the region: there is a strong improvement in the agreement between model and
17 observations when biomass burning emissions are included in the model (Fig. 2b-d; NMBF =
18 0.62 to -0.25, $r^2=0.77-0.83$) relative to the simulation without fire emissions (Fig. 2a; NMBF=
19 -1.85, $r^2=0.44$).

20 The overall bias between model and observations is smallest with FINN1 emissions (NMBF=
21 -0.25) compared to GFED3 (NMBF= -0.49) or GFAS1 (NMBF= -0.62), with simulated
22 monthly mean concentrations mostly within a factor of ~2 of the observations. The correlation
23 between model and observations across all sites is relatively similar between the three
24 emission datasets, with a slightly stronger correlation with GFED3 emissions ($r^2=0.83$)
25 compared to FINN1 ($r^2=0.77$) and GFAS1 ($r^2=0.79$).

26 The NMBF and correlation between model and observations are shown for the individual
27 stations in Fig. 3a. Correlations are calculated between simulated and observed multi-annual
28 monthly mean concentrations to evaluate the ability of the model to simulate seasonal

1 variability in aerosol. In general, the model with fire emissions overestimates observed PM2.5
2 concentrations at the forest site near Manaus (mean NMBF=0.57) but underestimates
3 observed PM2.5 concentrations at the sites that are more strongly impacted by biomass
4 burning (Porto Velho, Alta Floresta and Santarem; mean NMBF= -0.60). Figure 3
5 demonstrates that the relatively small bias with the FINN1 emissions in Fig. 2 is partly due to
6 an overestimation of PM2.5 concentrations at Manaus (NMBF=0.98), but also due to smaller
7 model biases at the three other sites (-0.51 to -0.11) compared to GFED3 (-0.76 to -0.48) and
8 GFAS1 (-1.26 to -0.39).

9 Figure 4 shows the multi-annual average seasonal cycle in observed and simulated PM2.5
10 concentrations at the four measurement sites (the full time-series at each site is shown in Fig.
11 S1 in the supplementary material). The model with biomass burning emissions simulates the
12 observed seasonal variability in PM2.5 concentrations over the Amazon region, characterised
13 by high concentrations in the local dry season (between ~June to ~December depending on
14 the site) and relatively low concentrations in the wet season. At Porto Velho, Santarem and
15 Alta Floresta, the model underestimates observed PM2.5 concentrations during the dry season
16 and has relatively good agreement during the wet season. This suggests that the negative
17 model bias in the dry season is largely due to uncertainty in the biomass burning emissions
18 rather than anthropogenic emissions, biogenic SOA or microphysical processes in the model.
19 The model overestimates PM2.5 concentrations observed at Manaus all year round, but
20 particularly during the dry season. This positive model bias may be due to several factors
21 including a possible overestimation of biogenic SOA over tropical forests and/or the model
22 resolution, which is not fully capturing the gradient in PM2.5 concentrations between the arc
23 of deforestation and the relatively undisturbed forest near Manaus.

24 In previous work we carried out a detailed model sensitivity analysis that accounted for the
25 uncertainty in the emissions (including biomass burning) and in the model processes such as
26 wet removal and dry deposition of aerosol (Lee et al., 2013). This analysis confirms that the
27 parametric uncertainty in modelled PM2.5 concentrations at these four stations is dominated
28 by the uncertainty in the biomass burning emissions flux in the dry season and by the yield of
29 biogenic SOA in the wet season, rather than the removal processes in the model.

30 Figure 4 demonstrates the differences in the spatial and temporal variability between the three
31 fire emission datasets, with different emissions capturing the observations better in different
32 months and locations. The model with GFED3 emissions captures the average seasonal
33 variability in PM2.5 observed at Alta Floresta (Fig. 4; $r^2=0.69$) and Porto Velho ($r^2=0.94$)

1 reasonably well. In particular, better simulating the peak in dry season concentrations at Porto
2 Velho than both FINN1 ($r^2=0.72$) and GFAS1 ($r^2=0.85$) emissions. However, PM_{2.5}
3 concentrations observed towards the end of the biomass burning season at Alta Floresta
4 (September – November) and Porto Velho (October – November) are not well captured by
5 GFED3 emissions, leading to larger biases at these sites (NMBF= -0.73 and -0.48,
6 respectively) than with FINN1 emissions (-0.51 and -0.41, respectively). At Santarem, the
7 model with GFED3 emissions underestimates observed PM_{2.5} concentrations throughout the
8 dry season, leading to a relatively large model bias and poor correlation with the observations
9 (NMBF= -0.76, $r^2=0.39$). Agreement with the observations at this site is improved with either
10 FINN1 (NMBF= -0.11, $r^2= 0.76$) or GFAS1 (NMBF= -0.39, $r^2= 0.75$) emissions (discussed
11 further in Sect. 4.2).

12 If we consider the inter-annual variability in simulated and observed PM_{2.5} concentrations
13 (Figure S2), we find that the results are consistent with the evaluation of the simulated
14 seasonal cycle. The smallest bias between model and observations is with the FINN1
15 emissions (NMBF= -0.22) compared to GFED3 (NMBF= -0.36) or GFAS1 (NMBF= -0.48).
16 One notable point is that the model with GFED3 emissions simulates the highest PM_{2.5}
17 concentrations for the 2010 drought year, relative to the model with GFAS1 or FINN1
18 emissions, leading to improved agreement with observations at Porto Velho (see Figs. 3a, 4a
19 and S2).

20 In summary, the model captures the seasonal cycle and inter-annual variability of observed
21 PM_{2.5} reasonably well at biomass burning influenced sites in the Amazon. However, the
22 model underestimates observed concentrations in the dry season suggesting that the biomass
23 burning aerosol emission fluxes in all three emission inventories (GFED3, FINN1, GFAS1)
24 may be underestimated. We explore this further in Section 4.3.

25 **4.1.2 Aerosol optical depth in tropical biomass burning regions**

26 Figure 5 shows the simulated versus observed multi-annual monthly mean AOD at 440 nm at
27 each of the AERONET sites displayed in Fig. 1 (simulated and observed annual means are
28 compared in Fig. S3). Agreement between model and observed AOD is improved
29 substantially when biomass burning emissions are included in the model (Fig 5; NMBF= -
30 0.40 to -0.18, $r^2=0.62-0.69$) compared to the simulation without fire emissions (NMBF= -
31 0.69, $r^2=0.22$). As for PM_{2.5}, the bias in AOD across all sites is smallest with the FINN1
32 emissions (NMBF= -0.18) compared to GFED3 (NMBF= -0.34) or GFAS1 (NMBF= -0.40).

1 The model with FINN1 emissions also shows slightly improved correlation with the
2 observations ($r^2=0.69$) relative to GFED3 ($r^2=0.67$) and GFAS1 ($r^2=0.62$).

3 Figure 6a shows the NMBF and correlation between simulated and observed multi-annual
4 monthly mean AOD at the individual AERONET sites, grouped by region. In South America,
5 the bias in modelled AOD is smallest with the FINN1 emissions (mean NMBF= -0.47)
6 compared to GFED3 (-0.69) and GFAS1 (-0.89) emissions, which is consistent with
7 comparisons between modelled and observed PM_{2.5} in Amazonia (Sect. 4.1.1). In Indochina,
8 the model with FINN1 emissions also gives the smallest bias (mean NMBF= -0.02), relative
9 to GFED3 (-0.21) and GFAS1 (-0.23). In Africa, the model bias is smallest with GFED3
10 emissions (mean NMBF= -0.78) compared to GFAS1 (-0.90) and FINN1 (-0.96). In
11 Equatorial Asia, the model bias is small and does not vary substantially between the different
12 emission datasets (FINN: 0.02, GFAS: -0.01, GFED: -0.02). In terms of temporal agreement
13 between model and observations, the correlation is noticeably stronger with GFED3 (mean r^2
14 =0.52) in Africa and with FINN1 (mean $r^2=0.75$) in Indochina, relative to the other emission
15 datasets.

16 In general, the model with fire emissions captures the seasonal variability in observed AOD
17 best in South America (mean $r^2=0.90$) and captures the magnitude of observed AOD best in
18 Southeast Asia (Equatorial Asia: mean NMBF= -0.00; Indochina: mean NMBF= -0.14). The
19 agreement between model and observations in Africa is relatively poor, with substantial
20 underestimation of observed AOD (mean NMBF= -0.88). The negative model bias in Africa
21 is unlikely to be solely due to an underestimation of biomass burning aerosol and is likely
22 complicated by a contribution from dust (Pandithurai et al., 2001; Sayer et al., 2014;
23 Cesnulyte et al., 2014; Queface et al., 2011). There is better agreement between the model and
24 observed AOD at Ascension Island, which observes aged biomass burning aerosol from the
25 African continent (Sayer et al., 2014), with all three emission inventories (mean NMBF= -
26 0.38, $r^2=0.84$). This suggests that the model is able to capture outflow of biomass burning
27 emissions from Africa.

28 At the South American sites located in regions of high biomass burning activity associated
29 with deforestation fires (Abracos Hill, Rio Branco, Ji Parana SE and Alta Floresta), there is a
30 small improvement in the correlation with observed AOD with FINN1 ($r^2=0.96-0.98$) and
31 GFAS1 ($r^2=0.94-0.97$) emissions relative to GFED3 ($r^2=0.79-0.88$). At these sites, AOD
32 observed at the tail end of the biomass burning season (~October-November) is better
33 captured by GFAS1 and FINN1 than GFED3, leading to the improved correlation relative to

1 GFED3. The model with GFED3 is generally better able to capture observed AOD at the peak
2 of the biomass burning season (~August-September) than GFAS1 and FINN, which is largely
3 due to relatively high GFED3 emission estimates for the drought years 2007 and 2010 (see
4 Fig. S1). These results are consistent with comparisons with observed PM_{2.5} concentrations
5 at Porto Velho and Alta Floresta (Sect. 4.1.1).

6 At the AERONET sites located in Equatorial Asia and the Philippines (Singapore, Bandung,
7 Manila Observatory, ND Marbel Univ) an improved performance of either the GFAS1 or
8 GFED3 emission inventories may be expected over FINN1 (Andela et al., 2013) due to their
9 improved representation of tropical peatlands (in Indonesia and Malaysian Borneo) in their
10 biome maps (van der Werf et al., 2010). The agreement between AOD observed at Bandung,
11 Indonesia and the model is marginally improved with GFED3 (NMBF= -0.14, $r^2=0.52$) or
12 GFAS1 (NMBF= -0.15, $r^2=0.47$) relative to FINN1 (NMBF= -0.18, $r^2=0.34$). However, at the
13 other sites we find no strong indication of an improved performance with GFED3 (NMBF= -
14 0.06 to 0.13, $r^2=0.15-0.24$) or GFAS1 (NMBF= -0.03 to 0.14, $r^2=0.13-0.56$) relative to FINN1
15 (NMBF= 0.04 to 0.17, $r^2=0.16-0.42$). At most of these sites the model does not simulate a
16 strong contribution of biomass burning to AOD, likely due to their urban locations, which
17 may explain why we do not see a substantial difference in the performances of the three
18 emission datasets. Long-term ground-based retrievals of AOD located outside the influence of
19 urban environments are lacking in Equatorial Asia.

20 At the African AERONET sites, observed AODs are generally better captured by the model
21 with GFED3 emissions (mean NMBF= -0.78, $r^2=0.52$) than with FINN1 (mean NMBF= -
22 0.96, $r^2=0.35$) or GFAS1 (mean NMBF= -0.90, $r^2=0.41$) emissions. Andela et al. (2013)
23 report that the GFED3 emissions flux of carbon monoxide (CO) is higher than GFAS1 or
24 FINN1 for humid savannah regions, where the burned area product may observe more cloud
25 covered fires than active-fire detection. This feature may explain the improved simulation of
26 AOD with GFED3 over Africa. Andela et al. (2013) also report that the FINN1 emission
27 estimates of CO are lower than both GFED3 and GFAS1 in global savannah regions, with the
28 largest spatial deviation found in humid savannahs where fire size is large. This may suggest
29 that the assumed fire size in FINN1 for savannah fires (0.75 km²) could be too small for
30 humid savannah fires in Africa, contributing to an underestimation of AOD in this region.

1 **4.1.3 Overview of PM_{2.5} and AOD evaluation**

2 In the previous sections we have evaluated the model against ground based observations of
3 PM_{2.5} and AOD. In general, we find that the model is negatively biased against observations
4 in regions strongly influenced by biomass burning. However, the model bias in surface PM_{2.5}
5 concentrations is generally smaller than for AOD over South America, where observations of
6 both quantities are available ($NMBF_{PM_{2.5}} = -1.85$ to -0.25 , $NMBF_{AOD} = -2.38$ to -0.40 ; see Figs.
7 2 and S4). If we compare average model biases (with fires) in multi-annual monthly mean
8 PM_{2.5} and AOD (for 2003-2004) at locations where AERONET stations are in close
9 proximity to the PM_{2.5} measurement stations, we find a larger model bias in AOD at
10 Santarem/Belterra ($NMBF_{PM_{2.5}} = -0.61$, $NMBF_{AOD} = -1.15$), but the reverse at Alta Floresta
11 ($NMBF_{PM_{2.5}} = -0.64$, $NMBF_{AOD} = -0.42$).

12 These results suggest that although the negative model bias in PM_{2.5} and AOD may be partly
13 due to an underestimation of biomass burning aerosol emissions (due to uncertainties
14 associated with fire detection and subsequent calculations of emission fluxes), there are likely
15 to be other factors contributing to the model discrepancy in AOD that do not affect modelled
16 surface PM_{2.5} concentrations. These factors include uncertainties in the calculation of AOD
17 that are largely associated with assumptions made about the aerosol optical properties
18 (assumed refractive indices), mixing state (external/internal mixing) and hygroscopic growth
19 of the aerosol. We investigate the sensitivity of simulated AOD to these assumptions below.

20 As described in Sect. 3.2, to calculate AOD at 440 nm we use component-specific refractive
21 indices from Bellouin et al. (2011) for a wavelength of 468 nm ($1.500 - 0.000i$ for POM and
22 $1.750 - 0.452i$ for BC). To test the sensitivity of AOD to the choice of refractive indices, we
23 applied the refractive indices tested by Matichuk et al. (2007) for smoke aerosol ($1.54 -$
24 $0.025i$ calculated by Haywood et al. (2003) for young smoke aerosol over southern Africa;
25 $1.51 - 0.024i$ and $1.52 - 0.019i$ retrieved by an AERONET station, Ndola in Zambia, located
26 close to smoke sources) to the BC and POM components in our model., We find that the
27 modelled AOD is relatively insensitive to the choice of complex refractive index within the
28 range of values tested here (altering the magnitude of AOD by less than 5%), which is in
29 agreement with Matichuk et al. (2007). Although the range of refractive indices tested is
30 relatively narrow (Matichuk et al., 2007), this result suggests that uncertainty in the assumed
31 refractive indices is unlikely to explain the discrepancy in modelled AOD.

1 We also find that the modelled AOD is fairly insensitive to the mixing state assumption, with
2 limited difference in AOD between assuming optical properties derived from an external
3 mixture of aerosol species and an internal (volumetrically-averaged) mixture. Figure 7 shows
4 the simulated versus observed multi-annual monthly mean AOD at AERONET sites when
5 assuming external and internal mixing and indicates that the difference is less than 5%,
6 internal mixing generally yielding higher AOD at the AERONET site locations. However, we
7 note that the internal mixing assumption used in this study does not take into account the
8 lensing effects of coating BC with organic aerosol, which has been shown to interact with the
9 aerosol absorption in a non-linear way (Saleh et al., 2015).

10 As described in Sect. 3.2, the hygroscopic growth of the aerosol is calculated in the model
11 using the ZSR scheme. To test the sensitivity of AOD to aerosol hygroscopic growth, we
12 instead use the κ -Köhler water uptake scheme, based upon the Köhler equation with a single
13 hygroscopic parameter, κ , defining the water uptake for different chemical species (Petters
14 and Kreidenweis, 2007) (see description of method in Sect. S1 of the supplementary
15 material). For the SO_4 , sea spray and POM components in the model we used the mean values
16 of κ for ammonium sulphate, sodium chloride and organic aerosol for subsaturated air masses
17 (0.53, 1.12 and 0.07, respectively) from Petters and Kreidenweis (2007). BC is considered
18 entirely hydrophobic in this model when using this scheme. The κ value for POM is based
19 upon that of α -pinene six hours after emission and is likely to be a minimum value as
20 oxidation of organic aerosol as it ages will tend to increase the hygroscopicity further. A wide
21 range of κ values are reported in the literature for organic aerosol (~0.01-0.6; Petters and
22 Kreidenweis, 2007) and biomass burning particles (0.02-0.8; DeMott et al., 2009; Petters et
23 al., 2009).

24 Using the κ -Köhler scheme the water uptake is reduced relative to the ZSR scheme; reducing
25 the simulated AOD on average by a factor of 1.7 at AERONET sites (see Fig. 7). This large
26 reduction relative to ZSR is in part from the assumption that the SO_4^{2-} component behaves as
27 ammonium sulphate rather than the more hygroscopic sulphuric acid, and the reduced water
28 uptake for POM. Therefore, the ZSR and κ -Köhler AOD can be considered high and low
29 water uptake cases, respectively, and highlight the large uncertainty present in the AOD from
30 aerosol hygroscopicity. This result is confirmed by comparing simulated AOD and mass
31 extinction efficiencies for the two water uptake cases against observations and values from
32 other global aerosol models (see Sect. S2 and Table S2).

1 Another important factor that will also influence the calculated AOD is the spatial resolution
2 of the simulated aerosol and RH (used to calculate aerosol water uptake) fields. These fields
3 are on a relatively coarse spatial resolution and will not capture small scale (sub-grid)
4 variability in these quantities that may influence point location measurements from
5 AERONET stations. A higher resolution model would be required to test how sensitive the
6 simulated AOD is to the spatial resolution of the aerosol and RH fields and whether or not
7 increasing the resolution improves the agreement with observed AOD (and reduces the
8 discrepancy between the model performance in AOD and PM_{2.5}). Bian et al. (2009) showed
9 that increasing the resolution of the RH field from 2°x2.5° to 1°x1.25° can increase simulated
10 AOD by ~10% in biomass burning regions (improving agreement with observations), which
11 may partly explain the larger discrepancies in AOD than PM_{2.5}.

12 Errors may also exist in the model representation of biomass burning aerosol, for example in
13 the modelled particle size distribution, that the simulated PM_{2.5} concentrations will be
14 relatively insensitive to but that will have implications for the simulated optical properties of
15 the aerosol and thus affect the calculated AOD. In addition, since AOD is a column-integrated
16 quantity, an underestimation of AOD may be due to an underestimation of aerosol
17 concentrations aloft since we have shown that the model agrees relatively well with PM_{2.5}
18 concentrations observed at the surface.

19 Further uncertainties in the model representation of biomass burning aerosol are associated
20 with the conversion of OC to organic matter (OM), which would affect both PM_{2.5}
21 concentrations and AOD predicted by the model. Increasing the assumed OM:OC ratio would
22 increase the total simulated mass of biomass burning aerosol. In our model we assume a
23 relatively low OM:OC ratio of 1.4 compared to previous studies on biomass burning aerosol.
24 Kaiser et al. (2012) use a value of 1.5, but note this ratio is low compared to values of around
25 2.2 proposed for aged pollution and biomass burning aerosols by Turpin and Lim (2001),
26 Pang et al. (2006) and Chen and Yu (2007) and a value of 2.6 used by Myhre et al. (2003) for
27 biomass burning aerosol in southern Africa. These larger OM:OC ratios could account for in-
28 plume (sub-grid) atmospheric oxidation and subsequent SOA formation observed in some
29 biomass burning plumes (Vakkari et al., 2014). In future work we need to include the
30 formation of semi-volatile SOA in biomass burning plumes that has been shown to be
31 important (Konovalov et al., 2015; Shrivastava et al., 2015).

1 **4.2 Small-scale fires**

2 The GFED3 fire emissions are known to underestimate contributions from small-scale fires
3 (smaller than ~100 ha) that are below the detection limit of the global burned area product
4 derived from MODIS (Randerson et al., 2012). However, many of these small fires generate
5 thermal anomalies that can be detected by satellites (Randerson et al., 2012). This means that
6 fire inventories using active fire detections to derive emissions (FINN1 and GFAS1) will
7 better capture these small fires (Kaiser et al., 2012). Kaiser et al. (2012) demonstrate that
8 GFAS1 includes emissions from small fires that are omitted in GFED3. Some of the
9 differences between the spatial patterns of emissions seen in Fig. 1 are likely due to missing
10 small fires in GFED3.

11 This result is corroborated by our comparisons between modelled and observed PM_{2.5}
12 concentrations at Santarem in the north region of Brazil (Sect. 4.1.1), where the poor
13 agreement between the observations and model with GFED3 emissions (NMBF= -0.76,
14 $r^2=0.39$) is substantially improved by using either of the active-fire based emission inventories
15 (FINN: NMBF= -0.11, $r^2= 0.76$; or GFAS: NMBF= -0.39, $r^2= 0.75$). Randerson et al. (2012)
16 show that in the region surrounding the Santarem station there is a particularly high small fire
17 fraction of total burned area, which explains why the GFED3 emissions do not capture the
18 observations in this region of Brazil. This result is consistent with comparisons between
19 modelled and observed AOD at the nearby AERONET station, Belterra. At this station, the
20 model better captures the observed AOD with either FINN1 (NMBF= -0.85, $r^2=0.84$) or
21 GFAS1 (NMBF= -1.02, $r^2=0.81$) emissions than with GFED3 emissions (NMBF= -1.58,
22 $r^2=0.29$).

23 The improved representation of small fire emissions in FINN1 and GFAS1 may also explain
24 the improved agreement between modelled and observed PM_{2.5} (Sect. 4.1.1) and AOD (Sect.
25 4.1.2) towards the end of the burning season (~October-November) in Amazonia. Kaiser et al.
26 (2012) report that GFAS1 exhibits slightly longer fire seasons in South America than GFED3.
27 Fires occurring at the tail end of the biomass burning season may be smaller in size and thus
28 better captured by using an active-fire based emission inventory (GFAS1 and FINN1
29 emissions). While at the peak of the burning season in Amazonia, when fires are potentially
30 larger, the comparisons in Sects. 4.1.1 and 4.1.2 suggest that GFED3 emissions capture the
31 observations better than FINN1 or GFAS1.

1 In Indochina, there is improved agreement between simulated and observed AOD with
2 FINN1 emissions (Fig. 6a; NMBF= -0.26 to 0.19, $r^2=0.14-0.98$) relative to both GFED3
3 (NMBF= -0.54 to -0.08, $r^2=0.11-0.84$) and GFAS1 (NMBF= -0.51 to -0.08, $r^2=0.03-0.83$).
4 Figure 8 compares the model with different emissions against observations at the nine
5 AERONET sites in Indochina. FINN1 emissions lead to an improved correlation with
6 observations at all sites and a reduced root mean square model error at six sites compared to
7 GFED3 and GFAS1. Figure 9 compares the multi-annual average seasonal cycle in AOD at
8 four sites in Thailand. The model with GFED3 and GFAS1 emissions underestimates AOD
9 observed during the dry season (~January – May), whereas the model with FINN1 emissions
10 captures the magnitude of dry season AOD reasonably well.

11 AERONET sites in Indochina (located in north and central Thailand and Vietnam) are
12 influenced by local agricultural burning (Li et al., 2013; Lin et al., 2013; Sayer et al., 2014) of
13 sugarcane and rice crop residues (Gadde et al., 2009; Sornpoon et al., 2014). Agricultural fires
14 are typically smaller than other fire types (e.g., deforestation, grassland/savannah and forest),
15 with burned areas of ~0.3 to ~16 ha reported for individual agricultural fires in the US
16 (McCarty et al., 2009) and Africa (Eva and Lambin, 1998). The prevalence of small fires in
17 Indochina may explain why FINN1 emissions result in better prediction of AOD compared to
18 GFED3 in this region.

19 We do not find an improved prediction of AOD with GFAS1 compared to GFED3 in this
20 region, although this would be expected since GFAS1 better captures emissions from small
21 fires than GFED3 (Kaiser et al., 2012). However, the GFAS1 FRP is converted to dry matter
22 burned using GFED3 data (Heil et al., 2010; Kaiser et al., 2012), which may lead to an
23 underestimation of small fire emissions in some regions. Conversely, FINN1 assumes a
24 relatively large burned area of 1 km² (100 ha) for individual agricultural fires and therefore
25 may overestimate emission fluxes in agricultural fire regions. However, since many small
26 fires may be undetected as fire hotspots by MODIS (due to factors such as the small size of
27 the fires, orbital gaps, persistent cloud cover and the timing of satellite overpass i.e. the
28 potential to miss fires events), by oversizing the area of individual burns, the FINN1
29 emissions may compensate for missing fire detections in this region (B. Yokelson, personal
30 communication, 2014).

1 **4.3 Scaling biomass burning emissions**

2 Previous model simulations, summarised in Table 2, underestimate AOD in regions impacted
3 by biomass burning. To improve simulation of AOD, these studies have scaled particulate
4 emissions from biomass burning (or aerosol concentrations) by a factor of 1.02 to 6. We have
5 found that our model with three different fire emission datasets also underestimates both
6 PM_{2.5} and AOD across tropical regions (although to a lesser extent in Southeast Asia). In this
7 section we explore the impact of scaling biomass burning emissions on simulated AOD and
8 PM_{2.5} concentrations. We performed two sensitivity simulations with each emission
9 inventory where we perturbed the biomass burning emission fluxes of BC and POM upwards
10 by factors of 1.5 and 3.4 (as recommended for GFED3 and GFAS1 by Kaiser et al. (2012)).

11 Figures 3b and 3c show the NMBF and correlation between simulated and observed multi-
12 annual monthly mean PM_{2.5} concentrations for the two simulations with scaled biomass
13 burning emissions. The outcome of scaling the emissions by a factor of 1.5 depends on the
14 site location. At the sites strongly impacted by biomass burning, the model bias in PM_{2.5} is
15 reduced (FINNx1.5: -0.16 to 0.08; GFEDx1.5: -0.67 to -0.15; GFASx1.5: -0.89 to -0.22) with
16 little change in the correlation. At the preserved forest site near Manaus, the positive model
17 bias is increased (FINNx1.5: 1.33; GFASx1.5: 0.69; GFEDx1.5: 0.66). The outcome of
18 scaling the emissions by a factor of 3.4 depends on both the site location and the emission
19 dataset. The model bias is increased at all sites with FINN1 emissions (0.63-2.72), with mixed
20 results for GFED3 (-0.39 to 1.18) and GFAS1 (-0.16 to 1.25) emissions. Any scaling of the
21 emissions leads to an overestimation of PM_{2.5} at Manaus with all three emission datasets.

22 In summary, a scaling factor of 1.5 applied to the FINN1 emissions is adequate for the model
23 to capture surface PM_{2.5} concentrations observed in regions of high fire activity in the
24 Amazon region. In contrast, the GFAS1 emissions require a larger scaling factor (closer to
25 3.4) for the model to capture surface PM_{2.5} observed at these sites.

26 The results of scaling the GFED3 emissions are more complex. Scaling GFED3 emissions by
27 a factor of 1.5, the model bias becomes relatively small at Alta Floresta (-0.36) and Porto
28 Velho (-0.15) but remains large and negative at Santarem (-0.67). Scaling the emissions by a
29 factor of 3.4 reduces the model bias at Santarem (-0.39), but leads to an overestimation of
30 PM_{2.5} at the other three sites (0.33-1.18). At Santarem, scaling GFED3 emissions by a factor
31 3.4 only marginally improves agreement with the observations; the correlation remains below
32 0.5 and model bias remains negative (despite a positive model bias at the other sites). This is

1 because GFED3 emission fluxes in the peak biomass burning season months in the region of
2 Santarem (November and December) are very low or non-existent, likely due to an omission
3 of small fires (Sect. 4.2), thus there are very few emissions to scale. This result suggests that
4 even by scaling GFED3 emissions by a large factor it is still possible to underestimate PM
5 from fires in regions influenced by emissions from small fires.

6 Figures 6a and 6b show the NMBF and correlation between simulated and observed multi-
7 annual monthly mean AOD with scaled biomass burning emissions. For the model with
8 GFAS1 emissions, scaling by a factor of 3.4 reduces the model bias at all but one site in
9 Indochina, Africa and South America (relative to the simulations without scaling or with a
10 scaling factor of 1.5), resulting in the best overall match to observed AOD in these regions. In
11 Equatorial Asia the scaling required to capture observed AOD depends on the site location
12 (two sites require no scaling and two sites require a scaling factor of either 1.5 or 3.4).

13 For GFED3 emissions, scaling by a factor of 3.4 results in the best overall match to observed
14 AOD in Africa and Indochina, but leads to an increased model bias at half the sites in South
15 America. However, even with a scaling factor of 3.4, the model with GFED3 emissions
16 continues to underestimate observed AOD in north Brazil (Belterra; NMBF= -0.94),
17 indicating that a large scaling factor does not fully compensate for the likely omission of
18 small fire emissions in this inventory (Sect. 4.2). The overall result of scaling GFED3
19 emissions in Equatorial Asia is the same for GFAS1 emissions.

20 Scaling FINN1 emissions by a factor of 3.4 improves the agreement with observed AOD in
21 Africa (at all sites), but generally leads to overestimation and increased model bias at sites in
22 South America and Southeast Asia. Scaling FINN1 emissions by a factor of 1.5 is adequate to
23 capture observed AOD at the majority of sites in South America (mean NMBF= -0.16), with
24 no scaling required for the majority of sites in Indochina (mean NMBF= 0.02) and Equatorial
25 Asia (mean NMBF= 0.02).

26 We note that even with a scaling factor of 3.4 applied to the biomass burning emissions, the
27 model underestimates observed AOD at the African AERONET sites with all three fire
28 emission inventories (mean NMBF= -0.31). This may indicate that a larger scaling factor is
29 required to capture observations in this region. However, using a too high scaling factor is
30 likely to compensate for model error e.g. too efficient removal of aerosol or underestimation
31 of dust emissions, and therefore overestimate the contribution of biomass burning to AOD.
32 The potential for compensation errors with emission scaling is relevant for all three regions.

1 For example, in South America the model bias in AOD in the wet season (~December to
2 May) is increased at four or more sites when the FINN1, GFED3, and GFAS1 emissions are
3 scaled by a factor of 3.4, which may be an indication of compensation errors. Compensation
4 errors are also likely to be occurring when emissions are scaled by a factor of 3.4 at sites in
5 urban locations (see Table S1 for location classifications), where a global model is unable to
6 capture sub-grid-scale urban emissions.

7 **5. Conclusions**

8 We have used the GLOMAP global aerosol model evaluated against surface PM2.5
9 observations and AERONET AOD to better understand the impacts of fires on tropical
10 aerosol. We compared three different satellite-derived fire emission datasets (GFED3, GFAS1
11 and FINN1). Total pan-tropical particulate emission (BC+OC) varied by less than 30%
12 between the different emission datasets. Regional differences were much larger (often
13 exceeding 100%) leading to important differences in aerosol concentrations simulated by the
14 global model.

15 We found that GLOMAP underestimated both PM2.5 and AOD in regions strongly impacted
16 by biomass burning, with all emission datasets. The largest underestimation of AOD occurred
17 across Africa, which may be partly due to a large contribution of dust. The smallest
18 underestimation of AOD occurred over Equatorial Asia, where the contribution of fire
19 emissions to simulated AOD was also smallest. Overall, the smallest bias between model and
20 both PM2.5 and AOD observations was found using FINN1 emissions. The model with
21 FINN1 emissions also best simulated the seasonal variability of AOD over Indochina,
22 potentially because of the dominance of smaller fires in this region that are better captured by
23 the FINN1 dataset.

24 In South America where we have coincident surface PM2.5 and AOD observations,
25 underestimation of AOD is greater than underestimation of surface PM2.5 in some locations.
26 We suggest this discrepancy could be caused by errors in i) vertical profile of aerosol, ii)
27 aerosol optical properties, size distribution and hygroscopic growth, or iii) model spatial
28 resolution. In particular, we find that simulated AOD is very sensitive to the calculation of
29 hygroscopic growth, with the magnitude of AOD ranging by a factor of ~1.7 between upper
30 and lower estimates. Detailed vertical profiles of aerosol properties over regions impacted by
31 fires are required to understand and resolve these issues. We caution against using AOD to
32 scale emissions before these issues are fully understood.

1 Particulate emissions from biomass burning are very uncertain with previous studies
2 underestimating AOD in regions impacted by fires and scaling particulate emissions by up to
3 a factor of 6 to help match observations (see Table 2). For each emission dataset we ran two
4 additional simulations where we scaled emissions up by factors of 1.5 and 3.4. We find that
5 the scaling that results in the best agreement with observations is regionally variable and
6 depends on the emission dataset used. With FINN1 emissions, PM_{2.5} concentrations and
7 AOD in South America are well simulated when emissions are increased by 50%, whereas
8 AOD in Africa is more consistent with a factor 3.4 scaling. In Southeast Asia, observed AOD
9 is well simulated without any scaling applied; scaling FINN1 emissions by 50% generally
10 leads to overestimation in this region. With GFAS1 emissions, PM_{2.5} concentrations in South
11 America and AOD in South America, Africa and Indochina are best simulated when
12 emissions are scaled by a factor 3.4. With GFED3 emissions, observations of PM_{2.5} in north
13 Brazil and AOD in Africa, Indochina and some regions of South America are also better
14 simulated with a factor 3.4 scaling; for PM_{2.5} concentrations and AOD observed in active
15 deforestation regions of South America, a 50% scaling is sufficient. In Equatorial Asia, the
16 results of scaling both GFAS1 and GFED3 emissions are mixed and depend on site location;
17 overall observed AOD is captured best either without scaling or with a scaling factor of 1.5.

18 A factor 1.5 scaling is within the uncertainty of emission datasets and is substantially smaller
19 than the emission scaling applied by many other studies (see Table 2). We also note that a
20 factor 1.5 scaling is within the uncertainty of assumed OM to OC ratios; we assume an
21 OM:OC ratio of 1.4 which is at the low end of other studies (Tsigaridis et al., 2014). Scaling
22 fire emissions by a factor of 3.4 to match AOD is likely to partly compensate for an
23 underestimation of aerosol from other sources e.g. dust and/or urban emissions and may also
24 compensate for errors in modelling of the aerosol distribution or calculation of AOD
25 (discussed above). In addition to these factors, we have treated biomass burning emissions as
26 primary and non-volatile. Formation of semi-volatile SOA in biomass burning plumes may be
27 important (Konovalov et al., 2015; Shrivastava et al., 2015) and needs to be explored in future
28 work.

29 Problems with the detection of small fires are an acknowledged issue for GFED3, which
30 relies on detections of area burned to derive emissions (Randerson et al., 2012). Over regions
31 that are likely dominated by small fires the model with GFED3 emissions substantially
32 underestimates both PM_{2.5} (north Brazil) and AOD (north Brazil and Thailand). The model
33 with GFAS1 and FINN1 emissions better simulates aerosol in these regions providing

1 independent evidence that these datasets better represent emissions from small fires. We note
2 that the most recent version of GFED emissions (GFED4) includes an estimate of emissions
3 from small fires (Giglio et al., 2013). Future work should evaluate these emissions against
4 aerosol observations to assess the representation of small fire emissions in the specific regions
5 highlighted here.

7 **Acknowledgements**

8 This research was supported by funding from the Natural Environment Research Council for
9 the South American Biomass Burning Analysis (SAMBBA) project (number NE/J009822/1).
10 The authors gratefully acknowledge the principal investigators (listed in Table S1) and their
11 staff responsible for establishing and maintaining the 27 AERONET stations used in this
12 study and providing quality-assured data.

14 **References**

- 15 Akagi, S. K., Yokelson, R. J., Wiedinmyer, C., Alvarado, M. J., Reid, J. S., Karl, T., Crouse,
16 J. D., and Wennberg, P. O.: Emission factors for open and domestic biomass burning for use
17 in atmospheric models, *Atmos. Chem. Phys.*, 11, 4039–4072, doi:10.5194/acp-11-4039-2011,
18 2011.
- 19 Al-Saadi, J., Soja, A., Pierce, R. B., Szykman, J., Wiedinmyer, C., Emmons, L., Kondragunta,
20 S., Zhang, X., Kittaka, C., Schaack, T., and Bowman, K.: Evaluation of near-real-time
21 biomass burning emissions estimates constrained by satellite fire data, *J. Appl. Remote Sens.*,
22 2, 021504, doi:10.1117/1.2948785, 2008.
- 23 Andela, N., Kaiser, J. W., Heil, A., van Leeuwen, T. T., van der Werf, G. R., Wooster, M. J.,
24 Remy, S. and Schultz, M. G.: Assessment of the Global Fire Assimilation System (GFASv1),
25 MACC-II Project Report, 2013.
- 26 Andreae, M. O. and Merlet, P.: Emission of trace gases and aerosols from biomass burning,
27 *Global Biogeochem. Cy.*, 15, 955–966, 2001.
- 28 Andreae, M. O., Rosenfeld, D., Artaxo, P., Costa, A. A., Frank, G. P., Longo, K. M., and
29 Silva-Dias, M. A. F.: Smoking rain clouds over the Amazon, *Science*, 303, 1337–1342,
30 doi:10.1126/science.1092779, 2004.
- 31 Arnold, S. R., Chipperfield, M. P., and Blitz, M. A.: A three dimensional model study of the
32 effect of new temperature dependent quantum yields for acetone photolysis, *J. Geophys. Res.*,
33 110, D22305, doi:10.1029/2005JD005998, 2005.
- 34 Artaxo, P., Rizzo, L. V., Brito, J. F., Barbosa, H. M. J., Arana, A., Sena, E. T., Cirino, G. G.,
35 Bastos, W., Martin, S. T., and Andreae, M. O.: Atmospheric aerosols in Amazonia and land
36 use change: From natural biogenic to biomass burning conditions, *Faraday Discuss.* 165, 203–
37 235, 2013.

- 1 Bauer, S. E., Menon, S., Koch, D., Bond, T. C., and Tsigaridis, K.: A global modeling study
2 on carbonaceous aerosol microphysical characteristics and radiative effects, *Atmos. Chem.*
3 *Phys.*, 10, 7439–7456, doi:10.5194/acp-10-7439-2010, 2010.
- 4 Bian, H., Chin, M., Rodriguez, J. M., Yu, H., Penner, J. E., and Strahan, S.: Sensitivity of
5 aerosol optical thickness and aerosol direct radiative effect to relative humidity, *Atmos.*
6 *Chem. Phys.*, 9, 2375-2386, doi:10.5194/acp-9-2375-2009, 2009.
- 7 Bistinas, I., Harrison, S. P., Prentice, I. C., and Pereira, J. M. C.: Causal relationships versus
8 emergent patterns in the global controls of fire frequency, *Biogeosciences*, 11, 5087-5101,
9 doi:10.5194/bg-11-5087-2014, 2014.
- 10 Bellouin, N., Rae, J., Jones, A. Johnson, C., Haywood, J. and Boucher, O.: Aerosol forcing in
11 the Climate Model Intercomparison Project (CMIP5) simulations by HadGEM2-ES and the
12 role of ammonium nitrate, *J. Geophys. Res.*, 116, D20206, doi:10.1029/2011JD016074, 2011.
- 13 Browse, J., Carslaw, K. S., Arnold, S. R., Pringle, K., and Boucher, O.: The scavenging
14 processes controlling the seasonal cycle in Arctic sulphate and black carbon aerosol, *Atmos.*
15 *Chem. Phys.*, 12, 6775-6798, doi:10.5194/acp-12-6775-2012, 2012.
- 16 Carlson, K. M., Curran, L. M., Ratnasari, D., Pittman, A. M., Soares-Filho, B. S., Asner, G.
17 P., Trigg, S. N., Gaveau, D. A., Lawrence, D. and Rodrigues, H. O.: Committed carbon
18 emissions, deforestation, and community land conversion from oil palm plantation expansion
19 in West Kalimantan, Indonesia. *Proc. Natl. Acad. Sci USA*, 109 (19), 7559-7564, 2012.
- 20 Carslaw, K. S., Lee, L. A., Reddington, C. L., Pringle, K. J., Rap, A., Forster, P. M., Mann, G.
21 W., Spracklen, D. V., Woodhouse, M. T., Regayre, J. R., and Pierce, L. A.: Large
22 contribution of natural aerosols to uncertainty in indirect forcing, *Nature*, 503.7474, 67–71,
23 2013.
- 24 Cesnulyte, V., Lindfors, A. V., Pitkänen, M. R. A., Lehtinen, K. E. J., Morcrette, J.-J., and
25 Arola, A.: Comparing ECMWF AOD with AERONET observations at visible and UV
26 wavelengths, *Atmos. Chem. Phys.*, 14, 593-608, doi:10.5194/acp-14-593-2014, 2014.
- 27 Chen, X. and Yu, J.: Measurement of organic mass to organic carbon ratio in ambient aerosol
28 samples using a gravimetric technique in combination with chemical analysis, *Atmos.*
29 *Environ.*, 41, 8857–8864, 2007.
- 30 Chew, B., Campbell, J., Reid, J., Giles, D., Welton, E., Salinas, S., and Liew, S.: Tropical
31 cirrus cloud contamination in sun photometer data, *Atmos. Environ.*, 45 (37), 6724–6731,
32 2011.
- 33 Chin, M., Diehl, T., Dubovik, O., Eck, T. F., Holben, B. N., Sinyuk, A., and Streets, D. G.:
34 Light absorption by pollution, dust, and biomass burning aerosols: a global model study and
35 evaluation with AERONET measurements, *Ann. Geophys.*, 27, 3439-3464,
36 doi:10.5194/angeo-27-3439-2009, 2009.
- 37 Chipperfield, M. P.: New version of the TOMCAT/SLIMCAT offline chemical transport
38 model: Intercomparison of stratospheric tracer experiments, *Q. J. Roy. Meteor. Soc.*, 132,
39 1179–1203, 2006.
- 40 Cochrane, M. A. and Laurance, W. F.: Fire as a large-scale edge effect in Amazonian forests,
41 *J. Trop. Ecol.*, 18, 311–325, 2002.
- 42 Cooke, W. F. and Wilson, J. J. N.: A global black carbon model, *J. Geophys. Res.*, 101,
43 19,395– 19,409, 1996.

1 Cox, P. M., Harris, P. P., Huntingford, C., Betts, R. A., Collins, M., Jones, C. D., Jupp, T. E.,
2 Marengo, J. A., and Nobre, C. A.: Increasing risk of Amazonian drought due to decreasing
3 aerosol pollution, *Nature*, 453, 212–216, doi:10.1038/nature06960, 2008.

4 Crutzen, P. J. and Andreae, M. O.: Biomass burning in the tropics: Impact on atmospheric
5 chemistry and biogeochemical cycles, *Science*, 250, 1669–1678, 1990.

6 Daskalakis, N., Myriokefalitakis, S., and Kanakidou, M.: Sensitivity of tropospheric loads and
7 lifetimes of short lived pollutants to fire emissions, *Atmos. Chem. Phys.*, 15, 3543–3563,
8 doi:10.5194/acp-15-3543-2015, 2015.

9 DeMott, P. J., Petters, M. D., Prenni, A. J., Carrico, C. M., Kreidenweis, S. M., Collett Jr., J.
10 L., and Moosmüller, H.: Ice nucleation behavior of biomass combustion particles at cirrus
11 temperatures, *J. Geophys. Res.*, 114, D16205, doi:10.1029/2009JD012036, 2009.

12 Dentener, F., Kinne, S., Bond, T., Boucher, O., Cofala, J., Generoso, S., Ginoux, P., Gong, S.,
13 Hoelzemann, J.J., Ito, A., Marelli, L., Penner, J.E., Putaud, J.-P., Textor, C., Schulz, M., van
14 der Werf, G.R., and Wilson, J.: Emissions of primary aerosol and precursor gases in the years
15 2000 and 1750 prescribed data-sets for AeroCom, *Atmos. Chem. Phys.*, 6, 4321–4344,
16 doi:10.5194/acp-6-4321-2006, 2006.

17 Doughty, C. E., Flanner, M. G., and Goulden, M. L.: Effect of smoke on subcanopy shaded
18 light, canopy temperature, and carbon dioxide uptake in an Amazon rainforest, *Global*
19 *Biogeochem. Cycles*, 24, GB3015, doi:10.1029/2009GB003670, 2010.

20 Emmanuel, S.C.: Impact to lung health of haze from forest fires: The Singapore experience,
21 *Respirology*, 5, 175–182, 2000.

22 Eva, H. and Lambin, E. F.: Remote sensing of biomass burning in tropical regions: Sampling
23 issues and multisensor approach, *Remote Sens. Environ.*, 64(3), 292–315, doi:10.1016/S0034-
24 4257(98)00006-6, 1998.

25 Feingold, G., Jiang, H., and Harrington, J. Y.: On smoke suppression of clouds in Amazonia,
26 *Geophys. Res. Lett.*, 32, L02804, doi:10.1029/2004GL021369, 2005.

27 Field, R. D., van der Werf, G. R., and Shen, S. S. P.: Human amplification of drought-induced
28 biomass burning in Indonesia since 1960, *Natl. Geosci.*, 2, 185–188, doi:10.1038/NGEO443,
29 2009.

30 Frankenberg, E., McKee, D. and Thomas, D.: Health consequences of forest fires in
31 Indonesia, *Demography*, 42, 109–129, 2005.

32 Gadde, B., Bonnet, S., Menke, C. and Garivait, S.: Air pollutant emissions from rice straw
33 open field burning in India, Thailand and the Philippines, *Environ. Pollut.*, 157, 1554–1558,
34 <http://dx.doi.org/10.1016/j.envpol.2009.01.004>, 2009.

35 Giglio, L.: MODIS Collection 4 Active Fire Product User's Guide Version 2.3, Science
36 Systems and Applications, Inc, 2005.

37 Giglio, L., Descloitres, J., Justice, C. O., Kaufman, Y. J.: An enhanced contextual fire
38 detection algorithm for MODIS. *Remote Sens. Environ.*, 87, 273–282, 2003.

39 Giglio, L., Randerson, J. T., van der Werf, G. R., Kasibhatla, P. S., Collatz, G. J., Morton, D.
40 C., and DeFries, R. S.: Assessing variability and long-term trends in burned area by merging
41 multiple satellite fire products, *Biogeosciences*, 7, 1171–1186, doi:10.5194/bg-7-1171-2010,
42 2010.

1 Giglio, L., Randerson, J. T., and van der Werf, G. R.: Analysis of daily, monthly, and annual
2 burned area using the fourth-generation global fire emissions database (GFED4) *J. Geophys.*
3 *Res. Biogeosci.*, 118, 317–328, doi:10.1002/jgrg.20042, 2013.

4 Golding, N. and Betts, R.: Fire risk in Amazonia due to climate change in the HadCM3
5 climate model: Potential interactions with deforestation, *Global Biogeochem. Cycles*, 22,
6 GB4007, doi:10.1029/2007GB003166, 2008.

7 Gonçalves, W. A., Machado, L. A. T., and Kirstetter, P.-E.: Influence of biomass aerosol on
8 precipitation over the Central Amazon: an observational study, *Atmos. Chem. Phys.*, 15,
9 6789-6800, doi:10.5194/acp-15-6789-2015, 2015.

10 Guenther, A., Hewitt, C. N., Erickson, D., Fall, R., Geron, C., Graedel, T., Harley, P.,
11 Klinger, L., Lerdau, M., McKay, W. A., Pierce, T., Scholes, B., Steinbrecher, R.,
12 Tallamraju, R., Taylor, J., and Zimmerman, P.: A global model of natural volatile organic
13 compound emissions, *J. Geophys. Res.*, 100(D5), 8873–8892, 1995.

14 Grainger, R. G., Lucas, J., Thomas, G. E., and Ewen, G. B. L.: Calculation of Mie
15 Derivatives, *Appl. Opt.*, 43, 5386, doi:10.1364/AO.43.005386, 2004.

16 Granier, C., Bessagnet, B., Bond, T., D'Angiola, A., Denier van der Gon, H., Frost, G. J.,
17 Heil, A., Kaiser, J. W., Kinne, S., Klimont, Z., Kloster, S., Lamarque, J.-F., Liousse, C.,
18 Masui, T., Meleux, F., Mieville, A., Ohara, T., Raut, J.-C., Riahi, K., Schultz, M. G., Smith,
19 S. J., Thompson, A., Aardenne, J., van der Werf, G. R., Vuuren, D. P.: Evolution of
20 anthropogenic and biomass burning emissions of air pollutants at global and regional scales
21 during the 1980–2010 period, *Clim. Change*, 109, 163–190, 2011.

22 Haywood, J. M., Osborne, S. R., Francis, P. N., Keil, A., Formenti, P., Andreae, M. O., and
23 Kaye, P. H.: The mean physical and optical properties of regional haze dominated by biomass
24 burning aerosol measured from the C-130 aircraft during SAFARI 2000, *J. Geophys. Res.*,
25 108(D13), 8473, doi:10.1029/2002JD002226, 2003.

26 Heald, C. L., and Spracklen, D. V.: Land use change impacts on air quality and climate,
27 *Chem. Rev.*, 115 (10), 4476-4496, doi: 10.1021/cr500446g, 2015.

28 Heil, A., Kaiser, J. W., van der Werf, G. R., Wooster, M. J., Schultz, M. G., and Denier van
29 der Gon, H.: Assessment of the Real-Time Fire Emissions (GFASv0) by MACC, Tech.
30 Memo. 628, ECMWF, Reading, UK, 2010.

31 Huang, K., Fu, J. S., Hsu, N. C., Gao, Y., Dong, X., Tsay, S.-C., and Lam, Y. F.: Impact
32 assessment of biomass burning on air quality in Southeast and East Asia during BASE-ASIA,
33 *Atmos. Environ.*, 78, 291-302, 2013.

34 Holben, B. N., Eck, T. F., Slutsker, I., Tanré, D., Buis, J. P., Setzer, A., Vermote, E., Reagan,
35 J. A., Kaufman, Y. J., Nakajima, T., Lavenue, F., Jankowiak, I., and Smirnov, A.:
36 AERONET—A Federated Instrument Network and Data Archive for Aerosol
37 Characterization, *Remote Sens. Environ.*, 66, 1, 1-16, [http://dx.doi.org/10.1016/S0034-](http://dx.doi.org/10.1016/S0034-4257(98)00031-5)
38 [4257\(98\)00031-5](http://dx.doi.org/10.1016/S0034-4257(98)00031-5), 1998.

39 Hoelzemann, J. J., Schultz, M. G., Brasseur, G. P., Granier, C., and Simon, M.: Global
40 Wildland Fire Emission Model (GWEM): evaluating the use of global area burnt satellite
41 data, *J. Geophys. Res.*, 109, D14S04, doi:10.1029/2003JD003666, 2004.

42 Ichoku, C. and Ellison, L.: Global top-down smoke-aerosol emissions estimation using
43 satellite fire radiative power measurements, *Atmos. Chem. Phys.*, 14, 6643-6667,
44 doi:10.5194/acp-14-6643-2014, 2014.

1 Ito, A. and Penner, J. E.: Global estimates of biomass burning emissions based on satellite
2 imagery for the year 2000, *J. Geophys. Res.*, 109, D14S05, doi:10.1029/2003JD004423,
3 2004.

4 Ito, A. and J. E. Penner: Estimates of CO emissions from open biomass burning in southern
5 Africa for the year 2000, *J. Geophys. Res.*, 110, D19306, doi:10.1029/2004JD005347, 2005.

6 Jacobson, M. Z., Effects of biomass burning on climate, accounting for heat and moisture
7 fluxes, black and brown carbon, and cloud absorption effects, *J. Geophys. Res. Atmos.*, 119,
8 8980–9002, doi:10.1002/2014JD021861, 2014.

9 Jacobson, L.d.S.V., Hacon, S.d.S., Castro, H.A.d., Ignotti, E., Artaxo, P., Saldiva, P.H.N.,
10 Leon, A.C.M. P.d.: Acute effects of particulate matter and black carbon from seasonal fires on
11 peak expiratory flow of schoolchildren in the Brazilian Amazon, *Plos One*, 9(8): e104177,
12 doi:10.1371/journal.pone.0104177, 2014.

13 Jathar, S. H., Gordon, T. D., Hennigan, C. J., Pye, H. O. T., Pouliot, G., Adams, P. J.,
14 Donahue, N. M., Robinson, A. L.: Unspeciated organic emissions from combustion sources
15 and their influence on the secondary organic aerosol budget in the United States. *Proc. Natl.*
16 *Acad. Sci USA*, 111(29), 10473-10478, 2014.

17 Johnson, B. T., Heese, B., McFarlane, S. A., Chazette, P., Jones, A., and Bellouin, N.:
18 Vertical distribution and radiative effects of mineral dust and biomass burning aerosol over
19 West Africa during DABEX, *J. Geophys. Res.*, 113, D00C12, doi:10.1029/2008JD009848,
20 2008.

21 Johnston, F. H., Henderson, S. B., Chen, Y., Randerson, J. T., Marlier, M., Defries, R. S.,
22 Kinney, P., Bowman, D. M. and Brauer, M.: Estimated global mortality attributable to smoke
23 from landscape fires, *Environ. Health Perspect.*, 120, 695-701, 2012.

24 Justice, C. O., Giglio, L., Korontzi, S., Owens, J., Morisette, J. T., Roy, D., Descloitres, J.,
25 Alleaume, S., Petitcolin, F., and Kaufman, Y.: The MODIS fire products, *RSE*, 83, 244–262,
26 2002.

27 Kaiser, J. W., Heil, A., Andreae, M. O., Benedetti, A., Chubarova, N., Jones, L., Morcrette,
28 J.-J., Razinger, M., Schultz, M. G., Suttie, M., and van der Werf, G. R.: Biomass burning
29 emissions estimated with a global fire assimilation system based on observations of fire
30 radiative power, *Biogeosciences*, 9, 527-554, doi:10.5194/bg-9-527-2012, 2012.

31 Kolusu, S. R., Marsham, J. H., Mulcahy, J., Johnson, B., Dunning, C., Bush, M., and
32 Spracklen, D. V.: Impacts of Amazonia biomass burning aerosols assessed from short-range
33 weather forecasts, *Atmos. Chem. Phys.*, 15, 12251-12266, doi:10.5194/acp-15-12251-2015,
34 2015.

35 Konovalov, I. B., Berezin, E. V., Ciais, P., Broquet, G., Beekmann, M., Hadji-Lazaro, J.,
36 Clerbaux, C., Andreae, M. O., Kaiser, J. W., and Schulze, E.-D.: Constraining CO₂ emissions
37 from open biomass burning by satellite observations of co-emitted species: a method and its
38 application to wildfires in Siberia, *Atmos. Chem. Phys.*, 14, 10383-10410, doi:10.5194/acp-
39 14-10383-2014, 2014.

40 Konovalov, I. B., Beekmann, M., Berezin, E. V., Petetin, H., Mielonen, T., Kuznetsova, I. N.,
41 and Andreae, M. O.: The role of semi-volatile organic compounds in the mesoscale evolution
42 of biomass burning aerosol: a modeling case study of the 2010 mega-fire event in Russia,
43 *Atmos. Chem. Phys.*, 15, 13269-13297, doi:10.5194/acp-15-13269-2015, 2015.

44 Lamarque, J.-F., Bond, T. C., Eyring, V., Granier, C., Heil, A., Klimont, Z., Lee, D., Liousse,
45 D., Mieville, A., Owen, B., Schultz, M. G., Shindell, D., Smith, S. J., Stehfest, E., Van

1 Aardenne, J., Cooper, O. R., Kainuma, M., Mahowald, N., McConnell, J. R., Naik, V., Riahi,
2 K., and van Vuuren, D. P.: Historical (1850-2000) gridded anthropogenic and biomass
3 burning emissions of ozone and aerosol precursors: methodology and application. *Atmos.*
4 *Chem. Phys.*, 10, 7017–7039, doi:10.5194/acp-10-7017-2010, 2010.

5 Lee, L. A., Pringle, K. J., Reddington, C. L., Mann, G. W., Stier, P., Spracklen, D. V., Pierce,
6 J. R., and Carslaw, K. S.: The magnitude and causes of uncertainty in global model
7 simulations of cloud condensation nuclei, *Atmos. Chem. Phys.*, 13, 8879-8914,
8 doi:10.5194/acp-13-8879-2013, 2013.

9 Li, C., Tsay, S.-C., Hsu, N. C., Kim, J. Y., Howell, S. G., Huebert, B. J., Ji, Q., Jeong, M.-J.,
10 Wang, S.-H., Hansell, R. A., and Bell, S. W.: Characteristics and composition of atmospheric
11 aerosols in Phimai, central Thailand during BASE-ASIA, *Atmos. Environ.*, 78, 60–71, 2013.

12 Lin, N.-H., Tsay, S.-C., Maring, H. B., Yen, M.-C., Sheu, G.-R., Wang, S.-H., Chi, K. H.,
13 Chuang, M.-T., Ou-Yang, C.-F., Fu, J. S., Reid, J. S., Lee, C.-T., Wang, L.-C., Wang, J.-L.,
14 Hsu, C. N., Sayer, A. M., Holben, B. N., Chu, Y.-C., Nguyen, X. A., Sopajaree, K., Chen, S.-
15 J., Cheng, M.-T., Tsuang, B.-J., Tsai, C.-J., Peng, C.-M., Schnell, R. C., Conway, T., Chang,
16 C.-T., Lin, K.-S., Tsai, Y. I., Lee, W.-J., Chang, S.-C., Liu, J.-J., Chiang, W.-L., Huang, S.-J.,
17 Lin, T.-H., and Liu, G.-R.: An overview of regional experiments on biomass burning aerosols
18 and related pollutants in Southeast Asia: From BASE-ASIA and the Dongsha Experiment to
19 7-SEAS, *Atmos. Environ.*, 78, 1–19, 2013.

20 Liousse, C., Penner, J. E., Chuang, C., Walton, J. J., Eddleman, H., and Cachier, H.: A global
21 three-dimensional model study of carbonaceous aerosols, *J. Geophys. Res.*, 101, 19411-
22 19432, 1996.

23 Liousse, C., Guillaume, B., Grégoire, J. M., Mallet, M., Galy, C., Pont, V., Akpo, A., Bedou,
24 M., Castéra, P., Dungall, L., Gardrat, E., Granier, C., Konaré, A., Malavelle, F., Mariscal, A.,
25 Mieville, A., Rosset, R., Serça, D., Solmon, F., Tummon, F., Assamoi, E., Yoboué, V., and
26 Van Velthoven, P.: Updated African biomass burning emission inventories in the framework
27 of the AMMA-IDAF program, with an evaluation of combustion aerosols, *Atmos. Chem.*
28 *Phys.*, 10, 9631-9646, doi:10.5194/acp-10-9631-2010, 2010.

29 Mann, G. W., Carslaw, K. S., Spracklen, D. V., Ridley, D. A., Manktelow, P. T.,
30 Chipperfield, M. P., Pickering, S. J., and Johnson, C. E.: Description and evaluation of
31 GLOMAP-mode: a modal global aerosol microphysics model for the UKCA composition-
32 climate model, *Geosci. Model Dev.*, 3, 519-551, doi:10.5194/gmd-3-519-2010, 2010.

33 Mann, G. W., Carslaw, K. S., Reddington, C. L., Pringle, K. J., Schulz, M., Asmi, A.,
34 Spracklen, D. V., Ridley, D. A., Woodhouse, M. T., Lee, L. A., Zhang, K., Ghan, S. J.,
35 Easter, R. C., Liu, X., Stier, P., Lee, Y. H., Adams, P. J., Tost, H., Lelieveld, J., Bauer, S. E.,
36 Tsigaridis, K., van Noije, T. P. C., Strunk, A., Vignati, E., Bellouin, N., Dalvi, M., Johnson,
37 C. E., Bergman, T., Kokkola, H., von Salzen, K., Yu, F., Luo, G., Petzold, A., Heintzenberg,
38 J., Clarke, A., Ogren, J. A., Gras, J., Baltensperger, U., Kaminski, U., Jennings, S. G.,
39 O'Dowd, C. D., Harrison, R. M., Beddows, D. C. S., Kulmala, M., Viisanen, Y., Ulevicius,
40 V., Mihalopoulos, N., Zdimal, V., Fiebig, M., Hansson, H.-C., Swietlicki, E., and Henzing, J.
41 S.: Intercomparison and evaluation of global aerosol microphysical properties among
42 AeroCom models of a range of complexity, *Atmos. Chem. Phys.*, 14, 4679-4713,
43 doi:10.5194/acp-14-4679-2014, 2014.

44 Marlier, M. E., DeFries, R. S., Voulgarakis, A., Kinney, P. L., Randerson, J. T., Shindell, D.
45 T., Chen, Y. and Faluvegi, G.: El Niño and health risks from landscape fire emissions in
46 southeast Asia, *Nature Clim. Change*, 3, 131-136, doi:10.1038/nclimate1658, 2013.

1 Matichuk, R. I., Colarco, P. R., Smith, J. A., and Toon, O. B.: Modeling the transport and
2 optical properties of smoke aerosols from African savanna fires during the Southern African
3 Regional Science Initiative campaign (SAFARI 2000), *J. Geophys. Res.*, 112, D08203,
4 doi:10.1029/2006JD007528, 2007.

5 Matichuk, R. I., Colarco, P. R., Smith, J. A. and Toon, O. B.: Modeling the transport and
6 optical properties of smoke plumes from South American biomass burning, *J. Geophys. Res.*,
7 113, D07208, doi:10.1029/2007JD009005, 2008.

8 McCarty, J. L., Korontzi, S., Justice, C. O., and Loboda, T.: The spatial and temporal
9 distribution of crop residue burning in the contiguous United States, *Sci. Total Environ.*,
10 407(21), 5701–5712, doi:10.1016/j.scitotenv.2009.07.009, 2009.

11 Malhi, Y., Aragão, L. E. O. C. , Galbraith, D., Huntingford, C., Fisher, R., Zelazowski, P.,
12 Sitch, S., McSweeney, C., and Meir, P.: Exploring the likelihood and mechanism of a climate-
13 change induced dieback of the Amazon rainforest, *P. Natl. Acad. Sci. USA*, 106, 20610–
14 20615, 2009.

15 Mu, M., Randerson, J. T., van der Werf, G. R., Giglio, L, Kasibhatla, P., Morton, D., Collatz,
16 G. J., DeFries, R. S., Hyer, E. J., Prins, E. M., Griffith, D. W. T., Wunch, D., Toon, G. C.,
17 Sherlock and V., Wennberg, P. O.: Daily and 3-hourly variability in global fire emissions and
18 consequences for atmospheric model predictions of carbon monoxide, *J. Geophys. Res.*, 116,
19 doi: 10.1029/2011JD016245, 2011.

20 Myhre, G., Berntsen, T. K., Haywood, J. M., Sundet, J. K., Holben, B. N., Johnsrud, M., and
21 Stordal, F.: Modeling the solar radiative impact of aerosols from biomass burning during the
22 Southern African Regional Science Initiative (SAFARI-2000) experiment, *J. Geophys. Res.*,
23 108(D13), 8501, doi:10.1029/2002JD002313, 2003.

24 Oliveira, P. H. F., Artaxo, P., Pires, C., De Lucca, S., Procopio, A., Holben, B., Schafer, J.,
25 Cardoso, L. F., Wofsy, S. C., and Rocha, H. R.: The effects of biomass burning aerosols and
26 clouds on the CO₂ flux in Amazonia, *Tellus B*, 59, 338–349, 2007.

27 Queface, A. J., Piketh, S. J., Eck, T. F., Tsay, S.-C. and Mavume, A.F.: Climatology of
28 aerosol optical properties in Southern Africa, *Atmos. Environ.*, 45, 2910-2921,
29 <http://dx.doi.org/10.1016/j.atmosenv.2011.01.056>, 2011.

30 Pandithurai, G., Pinker, R. T., Dubovik, O., Holben, B. N., and Aro, T.: Remote sensing of
31 aerosol optical characteristics in sub-Sahel, West Africa, *J. Geophys. Res.*, 106, 28347–
32 28356, doi:10.1029/2001JD900234, 2001.

33 Pang, Y., Turpin, B., and Gundel, L.: On the importance of organic oxygen for understanding
34 organic aerosol particles, *Aerosol Sci. Tech.*, 40, 128–133, 2006.

35 Petters, M. D. and Kreidenweis, S. M.: A single parameter representation of hygroscopic
36 growth and cloud condensation nucleus activity, *Atmos. Chem. Phys.*, 7, 1961–1971,
37 doi:10.5194/acp-7-1961-2007, 2007.

38 Petters, M. D., Carrico, C. M., Kreidenweis, S. M., Prenni, A. J., DeMott, P. J., Collett Jr., J.
39 L., and Moosmüller, H.: Cloud condensation nucleation activity of biomass burning aerosol,
40 *J. Geophys. Res.*, 114, D22205, doi:10.1029/2009JD012353, 2009.

41 Petrenko, M., Kahn, R., Chin, M., Soja, A., Kucsera, T., and Harshvardhan: The use of
42 satellite-measured aerosol optical depth to constrain biomass burning emissions source
43 strength in the global model GOCART, *J. Geophys. Res.*, 117, D18212,
44 doi:10.1029/2012JD017870, 2012.

- 1 Pierce, J. R. and Adams, P. J.: Uncertainty in global CCN concentrations from uncertain
2 aerosol nucleation and primary emission rates, *Atmos. Chem. Phys.*, 9, 1339–1356,
3 doi:10.5194/acp-9-1339-2009, 2009.
- 4 Pierce, J. R., Chen, K., and Adams, P. J.: Contribution of primary carbonaceous aerosol to
5 cloud condensation nuclei: processes and uncertainties evaluated with a global aerosol
6 microphysics model, *Atmos. Chem. Phys.*, 7, 5447–5466, doi:10.5194/acp-7-5447-2007,
7 2007.
- 8 Ramanathan, V., Crutzen, P. J., Kiehl, J. T., and Rosenfeld, D.: Aerosols, climate, and the
9 hydrological cycle, *Science*, 294, 2119–2124, 2001.
- 10 Randerson, J. T., Chen, Y., van der Werf, G. R., Rogers, B. M. and Morton, D. C.: Global
11 burned area and biomass burning emissions from small fires, *J. Geophys. Res.*, 117, G04,012,
12 doi:10.1029/2012JG002128, 2012.
- 13 Rap, A., Spracklen, D. V., Mercado, L., Reddington, C. L., Haywood, J. M., Ellis, R. J.,
14 Phillips, O. L., Artaxo, P., Bonal, D., Restrepo Coupe, N., and Butt, N.: Fires increase
15 Amazon forest productivity through increases in diffuse radiation, *Geophys. Res. Lett.*, 42,
16 4654–4662, doi:10.1002/2015GL063719, 2015.
- 17 Reddington, C. L., Carslaw, K. S., Spracklen, D. V., Frontoso, M. G., Collins, L., Merikanto,
18 J., Minikin, A., Hamburger, T., Coe, H., Kulmala, M., Aalto, P., Flentje, H., Plass-Dülmer,
19 C., Birmili, W., Wiedensohler, A., Wehner, B., Tuch, T., Sonntag, A., O'Dowd, C. D.,
20 Jennings, S. G., Dupuy, R., Baltensperger, U., Weingartner, E., Hansson, H.-C., Tunved, P.,
21 Laj, P., Sellegri, K., Boulon, J., Putaud, J.-P., Gruening, C., Swietlicki, E., Roldin, P.,
22 Henzing, J. S., Moerman, M., Mihalopoulos, N., Kouvarakis, G., Ždímal, V., Zíková, N.,
23 Marinoni, A., Bonasoni, P., and Duchi, R.: Primary versus secondary contributions to particle
24 number concentrations in the European boundary layer, *Atmos. Chem. Phys.*, 11, 12007-
25 12036, doi:10.5194/acp-11-12007-2011, 2011.
- 26 Reddington, C. L., McMeeking, G., Mann, G. W., Coe, H., Frontoso, M. G., Liu, D., Flynn,
27 M., Spracklen, D. V., and Carslaw, K. S.: The mass and number size distributions of black
28 carbon aerosol over Europe, *Atmos. Chem. Phys.*, 13, 4917-4939, doi:10.5194/acp-13-4917-
29 2013, 2013.
- 30 Reddington, C. L., Yoshioka M., Balasubramanian, R., Ridley, D., Toh, Y. Y., Arnold, S. R.,
31 and Spracklen, D. V.: Contribution of vegetation and peat fires to particulate air pollution in
32 Southeast Asia, *Environ. Res. Lett.*, 9, 094006, 2014.
- 33 Reddington, C. L., Butt, E. W., Ridley, D. A., Artaxo, P., Morgan, W. T., Coe, H., and
34 Spracklen, D. V.: Air quality and human health improvements from reductions in
35 deforestation-related fire in Brazil. *Nat Geosci.*, 8, 768–71, doi:10.1038/ngeo2535, 2015.
- 36 Reid, J. S., Koppmann, R., Eck, T. F., and Eleuterio, D. P.: A review of biomass burning
37 emissions part II: intensive physical properties of biomass burning particles, *Atmos. Chem.*
38 *Phys.*, 5, 799-825, doi:10.5194/acp-5-799-2005, 2005.
- 39 Reid, J. S., Hyer, E. J., Prins, E. M., Westphal, D. L., Zhang, J., Wang, J., Christopher, S. A.,
40 Curtis, C. A., Schmidt, C. C., Eleuterio, D. P., Richardson, K. A., and Hoffman, J. P.: Global
41 monitoring and forecasting of biomass-burning smoke: Description of and lessons from the
42 Fire Locating and Modeling of Burning Emissions (FLAMBE) Program, *IEEE J. Sel. Top.*
43 *Appl.*, 2, 3, 144–162, doi:10.1109/JSTARS.2009.2027443, 2009.

1 Rissler, J., Vestin, A., Swietlicki, E., Fisch, G., Zhou, J., Artaxo, P., and Andreae, M. O.: Size
2 distribution and hygroscopic properties of aerosol particles from dry-season biomass burning
3 in Amazonia, *Atmos. Chem. Phys.*, 6, 471-491, doi:10.5194/acp-6-471-2006, 2006.

4 Sakaeda, N., R. Wood, and P. J. Rasch: Direct and semidirect aerosol effects of southern
5 African biomass burning aerosol, *J. Geophys. Res.*, 116, D12205,
6 doi:10.1029/2010JD015540, 2011.

7 Sayer, A. M., Hsu, N. C., Eck, T. F., Smirnov, A., and Holben, B. N.: AERONET-based
8 models of smoke-dominated aerosol near source regions and transported over oceans, and
9 implications for satellite retrievals of aerosol optical depth, *Atmos. Chem. Phys.*, 14, 11493-
10 11523, doi:10.5194/acp-14-11493-2014, 2014.

11 Schmidt, A., Carslaw, K. S., Mann, G. W., Rap, A., Pringle, K. J., Spracklen, D. V., Wilson,
12 M., and Forster, P. M.: Importance of tropospheric volcanic aerosol for indirect radiative
13 forcing of climate, *Atmos. Chem. Phys.*, 12, 7321-7339, doi:10.5194/acp-12-7321-2012,
14 2012.

15 Schultz, M. G., Heil, A., Hoelzemann, J. J., Spessa, A., Thonicke, K., Goldammer, J. G.,
16 Held, A. C., Pereira, J. M. C., and van het Bolscher, M.: Global wildland fire emissions from
17 1960 to 2000, *Global Biogeochem. Cy.*, 22, GB2002, doi:10.1029/2007GB003031, 2008.

18 Scott, C. E., Rap, A., Spracklen, D. V., Forster, P. M., Carslaw, K. S., Mann, G. W., Pringle,
19 K. J., Kivekäs, N., Kulmala, M., Lihavainen, H., and Tunved, P.: The direct and indirect
20 radiative effects of biogenic secondary organic aerosol, *Atmos. Chem. Phys.*, 14, 447-470,
21 doi:10.5194/acp-14-447-2014, 2014.

22 Seiler, W. and Crutzen, P. J.: Estimates of gross and net fluxes of carbon between the
23 biosphere and the atmosphere from biomass burning. *Climatic Change*, 2(3):207–247, 1980.

24 Shrivastava, M., R. C. Easter, X. Liu, A. Zelenyuk, B. Singh, K. Zhang, P.-L. Ma, D. Chand,
25 S. Ghan, J. L. Jimenez, Q. Zhang, J. Fast, P. J. Rasch, and P. Tiitta: Global transformation and
26 fate of SOA: Implications of low-volatility SOA and gas-phase fragmentation reactions. *J.*
27 *Geophys. Res. Atmos.*, 120,4169–4195. doi: 10.1002/2014JD022563, 2015.

28 Sornpoon, W., Bonnet, S., Kasemsap, P., Prasertsak, P., Garivait, S.: Estimation of emissions
29 from sugarcane field burning in Thailand using bottom-up country-specific activity data,
30 *Atmosphere*, 5, 669-685, 2014.

31 Spracklen, D. V., Pringle, K. J., Carslaw, K. S., Chipperfield, M. P., and Mann, G. W.: A
32 global off-line model of size-resolved aerosol microphysics: I. Model development and
33 prediction of aerosol properties, *Atmos. Chem. Phys.*, 5, 2227-2252, doi:10.5194/acp-5-2227-
34 2005, 2005a.

35 Spracklen, D. V., Pringle, K. J., Carslaw, K. S., Chipperfield, M. P., and Mann, G. W.: A
36 global off-line model of size-resolved aerosol microphysics: II. Identification of key
37 uncertainties, *Atmos. Chem. Phys.*, 5, 3233-3250, doi:10.5194/acp-5-3233-2005, 2005b.

38 Spracklen, D. V., Carslaw, K. S., Kulmala, M., Kerminen, V.-M., Mann, G. W., and Sihto,
39 S.-L.: The contribution of boundary layer nucleation events to total particle concentrations
40 on regional and global scales, *Atmos. Chem. Phys.*, 6, 5631–5648, doi:10.5194/acp-6-5631-
41 2006, 2006.

42 Spracklen, D. V., Carslaw, K. S., Kulmala, M., Kerminen, V.-M., Sihto, S.-L., Riipinen, I.,
43 Merikanto, J., Mann, G. W., Chipperfield, M. P., Wiedensohler, A., Birmili, W., and
44 Lihavainen, H.: Contribution of particle formation to global cloud condensation nuclei
45 concentrations, *Geophys. Res. Lett.*, 35, L06808, doi:10.1029/2007GL033038, 2008

1 Spracklen, D. V., Jimenez, J. L., Carslaw, K. S., Worsnop, D. R., Evans, M. J., Mann, G. W.,
2 Zhang, Q., Canagaratna, M. R., Allan, J., Coe, H., McFiggans, G., Rap, A., and Forster, P.:
3 Aerosol mass spectrometer constraint on the global secondary organic aerosol budget, *Atmos.*
4 *Chem. Phys.*, 11, 12109–12136, doi:10.5194/acp-11-12109-2011, 2011a.

5 Spracklen, D. V., Carslaw, K. S., Poschl, U., Rap, A., and Forster, P. M.: Global cloud
6 condensation nuclei influenced by carbonaceous combustion aerosol, *Atmos. Chem. Phys.*,
7 11, 9067–9087, doi:10.5194/acp-11-9067-2011, 2011b.

8 Stokes, R. H. and Robinson, R. A.: Interactions in aqueous nonelectrolyte solutions. I. Solute-
9 solvent equilibria, *J. Phys. Chem.*, 70, 2126–2130, 1966.

10 Swap, R., Garstang, M., Macko, S. A., Tyson, P. D., Maenhaut, W., Artaxo, P., Kållberg, P.,
11 and Talbot, R.: The long-range transport of southern African aerosols to the tropical South
12 Atlantic, *J. Geophys. Res.*, 101(D19), 23777–23791, doi:10.1029/95JD01049, 1996.

13 Tosca, M. G., Randerson, J. T. and Zender, C. S.: Global impact of smoke aerosols from
14 landscape fires on climate and the Hadley circulation, *Atmos. Chem. Phys.*, 13, 5227–5241,
15 doi:10.5194/acp-13-5227-2013, 2013.

16 Tosca, M. G., Diner, D., Garay, M., and Kalashnikova, O.: Observational evidence of fire-
17 driven reduction of cloud fraction in tropical Africa, *J. Geophys. Res.*, 119, 8418–8432,
18 doi:10.1002/2014JD021759, 2014.

19 Tosca, M. G., Diner, D. J., Garay, M. J., and Kalashnikova, O. V.: Human-caused fires limit
20 convection in tropical Africa: First temporal observations and attribution, *Geophys. Res. Lett.*,
21 42, doi:10.1002/2015GL065063, 2015.

22 Tsigaridis, K., Daskalakis, N., Kanakidou, M., Adams, P. J., Artaxo, P., Bahadur, R.,
23 Balkanski, Y., Bauer, S. E., Bellouin, N., Benedetti, A., Bergman, T., Berntsen, T. K.,
24 Beukes, J. P., Bian, H., Carslaw, K. S., Chin, M., Curci, G., Diehl, T., Easter, R. C., Ghan, S.
25 J., Gong, S. L., Hodzic, A., Hoyle, C. R., Iversen, T., Jathar, S., Jimenez, J. L., Kaiser, J. W.,
26 Kirkevåg, A., Koch, D., Kokkola, H., Lee, Y. H., Lin, G., Liu, X., Luo, G., Ma, X., Mann, G.
27 W., Mihalopoulos, N., Morcrette, J.-J., Müller, J.-F., Myhre, G., Myriokefalitakis, S., Ng, N.
28 L., O'Donnell, D., Penner, J. E., Pozzoli, L., Pringle, K. J., Russell, L. M., Schulz, M., Sciare,
29 J., Seland, Ø., Shindell, D. T., Sillman, S., Skeie, R. B., Spracklen, D., Stavrakou, T.,
30 Steenrod, S. D., Takemura, T., Tiitta, P., Tilmes, S., Tost, H., van Noije, T., van Zyl, P. G.,
31 von Salzen, K., Yu, F., Wang, Z., Wang, Z., Zaveri, R. A., Zhang, H., Zhang, K., Zhang, Q.,
32 and Zhang, X.: The AeroCom evaluation and intercomparison of organic aerosol in global
33 models, *Atmos. Chem. Phys.*, 14, 10845–10895, doi:10.5194/acp-14-10845-2014, 2014.

34 Turpin, B. J. and Lim, H.-J.: Species contributions to PM_{2.5} mass concentrations: Revisiting
35 common assumptions for estimating organic mass, *Aerosol Sci. Tech.*, 36, 602–610, 2001.

36 Vakkari, V., Kerminen, V.-M., Beukes, J. P., Tiitta, P., van Zyl, P. G., Josipovic, M., Venter,
37 A. D., Jaars, K., Worsnop, D. R., Kulmala, M., and Laakso, L.: Rapid changes in biomass
38 burning aerosols by atmospheric oxidation, *Geophys. Res. Lett.*, 41, 2644–2651,
39 doi:10.1002/2014GL059396., 2014

40 Val Martin, M., Logan, J. A., Kahn, R. A., Leung, F.-Y. , Nelson, D. L. and Diner, D. J.:
41 Smoke injection heights from fires in North America: Analysis of 5 years of satellite
42 observations, *Atmos. Chem. Phys.*, 10, 1491–1510, doi:10.5194/acp-10-1491-2010, 2010.

43 van der Werf, G. R., Randerson, J. T., Collatz, G. J., and Giglio, L.: Carbon emissions from
44 fires in tropical and subtropical ecosystems, *Global Change Biol.*, 9, 547–562, 2003.

- 1 van der Werf, G. R., Randerson, J. T., Giglio, L., Collatz, G. J., Kasibhatla, P. S., and
2 Arellano, A. F.: Interannual variability in global biomass burning emissions from 1997 to
3 2004, *Atmos. Chem. Phys.*, 6, 3423–3441, doi:10.5194/acp-6-3523-2006, 2006.
- 4 van der Werf, G. R., Randerson, J. T., Giglio, L., Collatz, G. J., Mu, M., Kasibhatla, P. S.,
5 Morton, D. C., DeFries, R. S., Jin, Y., van Leeuwen, T. T.: Global fire emissions and the
6 contribution of deforestation, savanna, forest, agricultural, and peat fires (1997-2009), *Atmos.*
7 *Chem. Phys.*, 10, 11707-11735, doi:10.5194/acp-10-11707-2010, 2010.
- 8 Ward, D. S., Kloster, S., Mahowald, N. M., Rogers, B. M., Randerson, J. T., and Hess, P. G.:
9 The changing radiative forcing of fires: global model estimates for past, present and future,
10 *Atmos. Chem. Phys.*, 12, 10857-10886, doi:10.5194/acp-12-10857-2012, 2012.
- 11 Wiedinmyer, C., Quayle, B., Geron, C., Belote, A., McKenzie, D., Zhang, X., O'Neill, S., and
12 Wynne, K. K.: Estimating emissions from fires in North America for Air Quality Modeling,
13 *Atmos. Environ.*, 40, 3419–3432, 2006.
- 14 Wiedinmyer, C., Akagi, S. K., Yokelson, R. J., Emmons, L. K., Al-Saadi, J. A., Orlando, J. J.,
15 and Soja, A. J.: The Fire INventory from NCAR (FINN): a high resolution global model to
16 estimate the emissions from open burning, *Geosci. Model Dev.*, 4, 625-641,
17 doi:10.5194/gmd-4-625-2011, 2011.
- 18 Yu, S., Eder, B., Dennis, R., Chu, S.-H. and Schwartz, S. E.: New unbiased symmetric
19 metrics for evaluation of air quality models, *Atmosph. Sci. Lett.*, 7: 26–34. doi:
20 10.1002/asl.125, 2006.
- 21 Zhang, X., Kondragunta, S., Ram, J., Schmidt, C., and Huang, H.-C: Near-real-time global
22 biomass burning emissions product from geostationary satellite constellation, *J. Geophys.*
23 *Res.*, 117, D14201 doi:10.1029/2012JD017459, 2012.
- 24 Zhou, J. C., Swietlicki, E., Hansson, H. C., and Artaxo, P.: Submicrometer aerosol particle
25 size distribution and hygroscopic growth measured in the Amazon rain forest during the wet
26 season, *J. Geophys. Res.*, 107 (D20), 8055, doi:10.1029/2001JD000203, 2002.

1 **Table 1.** Summary of biomass burning emission inventories used in this study: the Global Fire
2 Emissions Database version 3 (GFED3), the National Centre for Atmospheric Research Fire Inventory
3 version 1.0 (FINN1) and the Global Fire Assimilation System version 1.0 (GFAS1). For each emission
4 inventory, the total amounts of black carbon (BC) and organic carbon (OC) aerosol emitted from fires
5 over the tropical region (defined as 23.5°N to 23.5°S) are given for the 2003 to 2011 average.
6 Numbers in parenthesis give the ratio to GFED3 emissions.

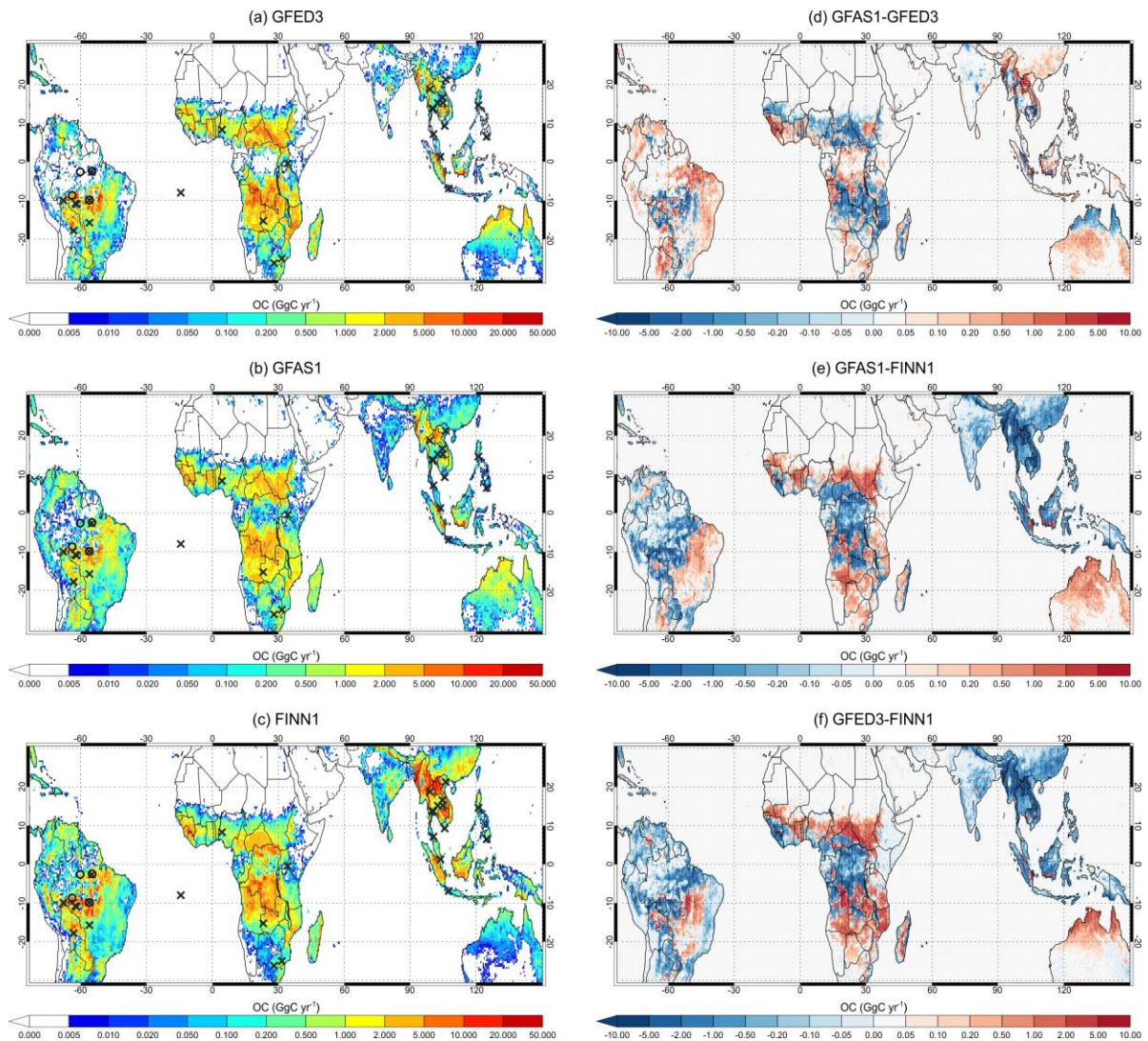
	GFED3	GFAS1	FINN1
Method	MODIS burned area & biogeochemical model	MODIS thermal anomaly product & fire radiative power	MODIS thermal anomaly product & assumed burned area
Spatial resolution	0.5° x 0.5°	0.5° x 0.5°	1 km x 1 km
Temporal resolution	Monthly (1997 – 2011) Daily (2003 – 2011)	Daily (2001 – 2015)	Daily (2002 – 2013)
Amount of OC emitted over tropics (Tg yr⁻¹)	13.412	11.731 (0.87)	17.282 (1.29)
Amount of BC emitted over tropics (Tg yr⁻¹)	1.705	1.532 (0.90)	1.724 (1.01)
OC:BC ratio over tropics	7.87	7.66	10.02
Reference	Van der Werf et al., 2010	Kaiser et al., 2012	Wiedinmyer et al., 2011

1 **Table 2.** Summary of scaling factors applied in previous modelling studies to biomass burning
2 emissions or modelled concentrations of biomass burning aerosol to match observations. Region
3 abbreviations used in the table are defined in van der Werf et al. (2006): Northern Hemisphere South
4 America (NHSA), Southern Hemisphere South America (SHSA), Northern Hemisphere Africa
5 (NHAF), Southern Hemisphere Africa (SHAF), Southeast Asia including the Philippines (SEAS) and
6 Equatorial Asia (EQAS). See van der Werf et al. (2006; 2010) for discussion of differences between
7 GFED versions 1, 2 and 3; on average GFED3 are 13% lower than GFED2 van der Werf et al. (2010),
8 with total GFED2 emissions lower than GFED1 in Central and Southern America and Southern Africa
9 (van der Werf et al., 2006).

10

Reference	Biomass burning emission inventory	Region of focus	Details of scaling applied
Myhre et al., 2003	Biomass burning BC emissions from the Global Emissions Inventory Activity (GEIA), based on Cooke and Wilson (1996); OC emissions from Liousse et al. (1996).	Southern Africa	Used a relatively high OM/OC ratio of 2.6 and increased the modelled aerosol mass by 20% to account for mass fraction of inorganic components observed to be of 17% of the total mass.
Matichuk et al., 2007	GFED1 (van der Werf et al., 2003)	Southern Africa	Multiple sensitivity studies were performed with the model including simulations with halved and doubled fire emissions..
Matichuk et al., 2008	GFED2 (van der Werf et al., 2006)	South America	Smoke source function was scaled up by a factor of 6..
Johnson et al., 2008	Biomass burning emissions following Dentener et al. (2006): GFED1 (van der Werf et al., 2004) for year 2000 or a 5-year (1997–2001) average (not specified)	West Africa	Increased mass concentration of biomass burning AOD by a factor of 2.4..
Chin et al., 2009	Calculated using dry mass burned dataset from GFED2 (van der Werf et al., 2006)	Global	No scaling applied, but used emission factors of BC (1 g kg ⁻¹) and OC (8 g kg ⁻¹) that are 40–100% higher than commonly used values (Andreae and Merlet, 2001).
Sakaeda et al., 2011	Aerosol fields taken from MATCH chemical transport model	Southern Africa	OC and BC masses were increased by a factor of 2 over 10°N–30°S and 20°W–50°E.
Johnston et al., 2012	GFED2 (van der Werf et al., 2006)	Global	Scalar adjustments made for 14 continental scale regions: NHSA (2.48-2.7), SHSA (1.9-3.3), NHAF (1.02-1.08), SHSA (1.68-2.01), SEAS (2.43-3.08), EQAS (2.3-2.72). Scaling factors were applied to modelled surface fire PM2.5 to match satellite observations of AOD (non-fire aerosol was also scaled).
Kaiser et al., 2012	GFED3 and GFASv1.0	Global	Model was biased low in South America and Africa by factors of 4.1 and 3.0. Recommended a global

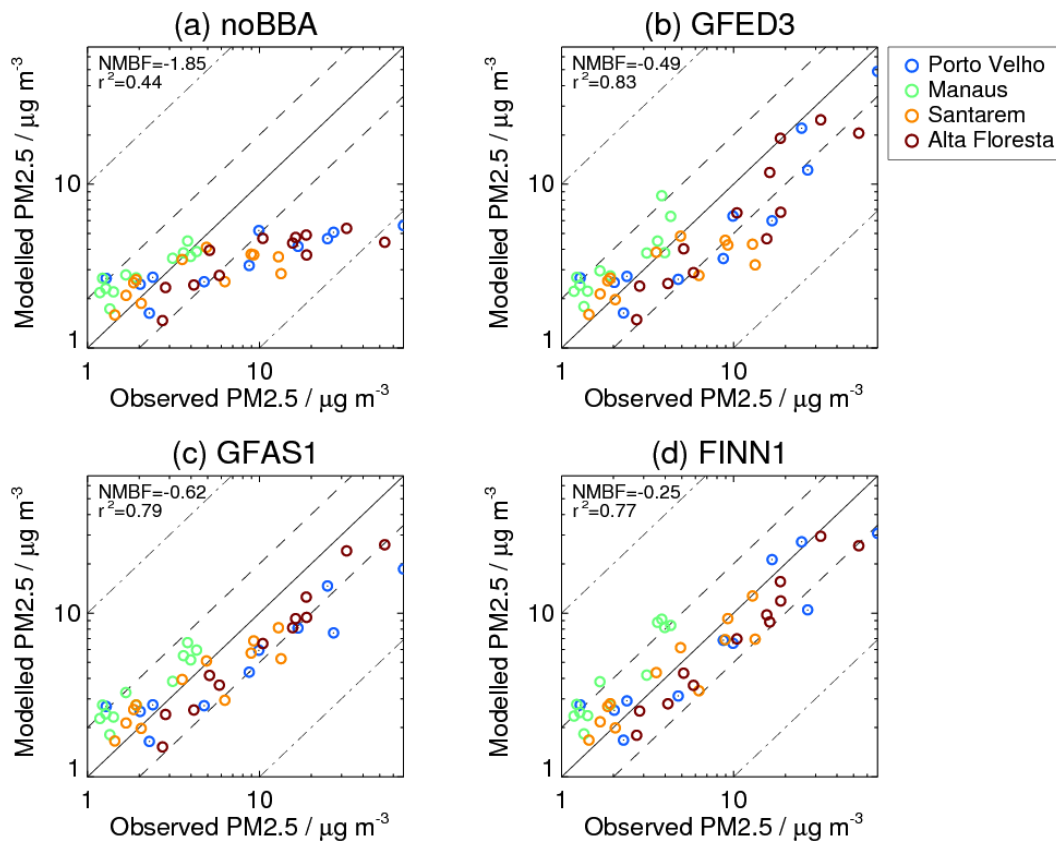
			enhancement of 3.4 for PM emissions from fires.
Ward et al., 2012	Calculated from Kloster et al. (2010, 2012) CLM3 simulations of global fire area burned; using emission factors from Andreae and Merlet (2001) and updates from Hoelzemann et al. (2004). Compared against GFED2.	Global	Scalar adjustments were made for continental scale regions following Johnston et al. (2012) with slight modifications: SHSA (2.0), NHAF (1.0), SHAF (3.0), SEAS (1.5), EQAS (3.0). Scaling factor directly applied to model fire emissions.
Tosca et al., 2013	GFED3	Global	Biomass burning BC and OC emissions scaled by factor of 2 globally with additional regional scaling factors applied: South America (2.4), Africa (2.1), Southeast Asia (1.67).
Marlier et al., 2013	GFED3	Southeast Asia	Total aerosol burden scaled by 1.02-1.96 (depending on model), with additional scaling factors of 1.36-2.26 applied to fire aerosol..



1

2 **Figure 1.** (a)-(c) Total annual emissions of organic carbon (OC) in $\text{Gg}(\text{C}) \text{ yr}^{-1}$ averaged over the
 3 period of January 2003 to December 2011 from (a) GFED3, (b) GFAS1 and (c) FINN1. Black circles
 4 mark the locations of the four aerosol measurement stations and black crosses mark the locations of
 5 the 27 AERONET stations (see Table S1). (d)-(f) Absolute difference in 2003-2011 mean annual OC
 6 emissions between GFAS1, GFED3 and FINN1 (d) GFAS1 minus GFED3 (e) GFAS1 minus FINN1
 7 (f) GFED3 minus FINN1. The FINN1 OC emissions (with a $1 \text{ km} \times 1 \text{ km}$ horizontal resolution) were
 8 aggregated onto a grid of $0.5^\circ \times 0.5^\circ$ degree resolution to compare with GFED3 and GFAS1.

9

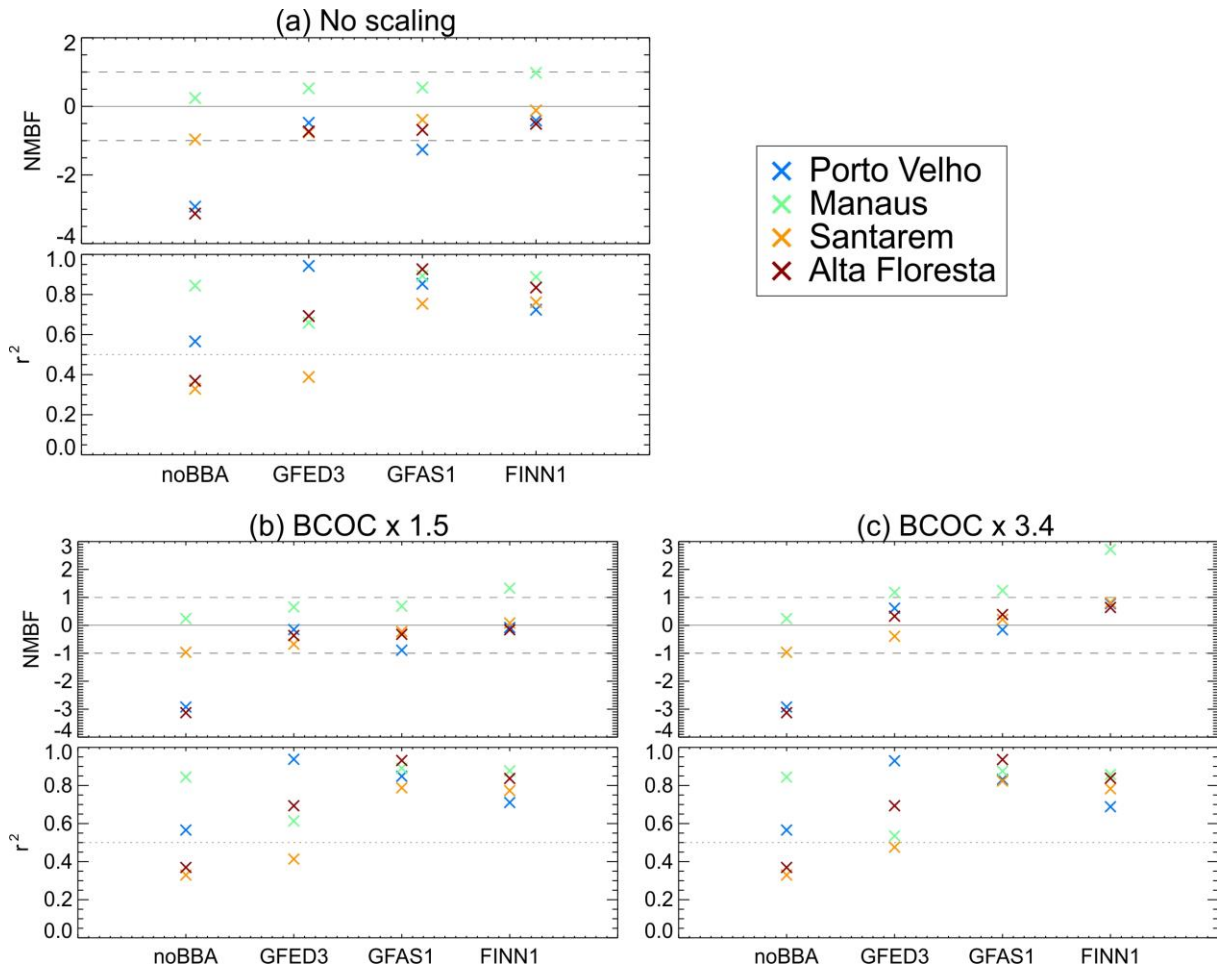


1

2 **Figure 2.** Simulated versus observed multi-annual monthly mean PM_{2.5} concentrations at each
 3 ground station in the Amazon region for the model (a) without biomass burning emissions, and with
 4 (b) GFED3, (c) GFAS1 and (d) FINN1 emissions. Multi-annual monthly mean concentrations were
 5 calculated by averaging over all years of data available between January 2003 and December 2011 to
 6 obtain an average seasonal cycle at each station. The normalised mean bias factor (NMBF; Yu et al.,
 7 2006) and Pearson's correlation (r^2) between modelled and observed PM_{2.5} concentrations are shown
 8 in the top left corner.

9

1

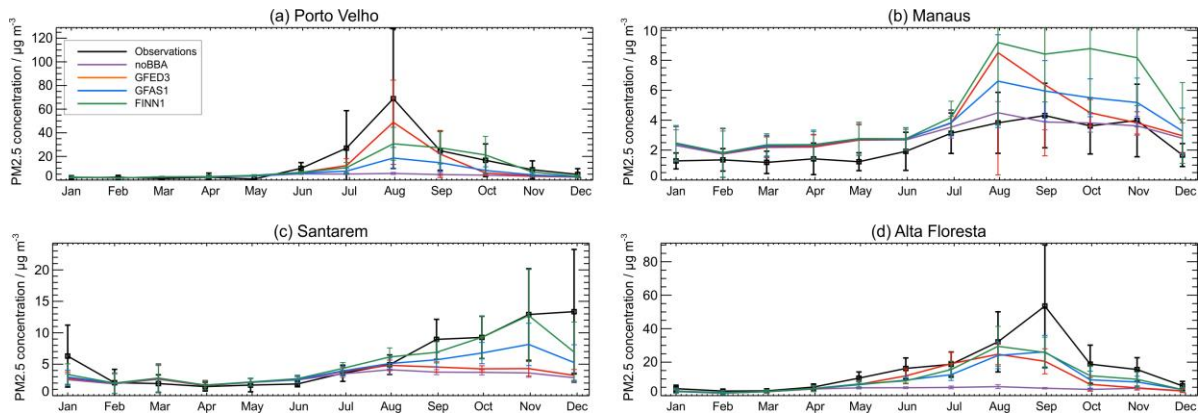


2

3 **Figure 3.** Normalised mean bias factor (NMBF; Yu et al., 2006) and Pearson's correlation coefficient
 4 (r^2) between modelled and observed multi-annual monthly-mean PM_{2.5} concentrations at each of the
 5 four ground stations in Amazonia. Results are shown for four model simulations: without fires
 6 (noBBA), and with each of the three biomass burning emissions inventories: GFED3, GFAS1, FINN1.
 7 (a) No scaling applied to the fire emissions; (b) particulate (BC/OC) fire emissions scaled up globally
 8 by a factor 1.5; (c) particulate (BC/OC) fire emissions scaled up globally by a factor of 3.4. The
 9 dashed lines indicate NMBFs of -1 and 1, which equate to an underestimation and overestimation,
 10 respectively, of a factor of 2. The dotted line indicates an r^2 value of 0.5.

11

12

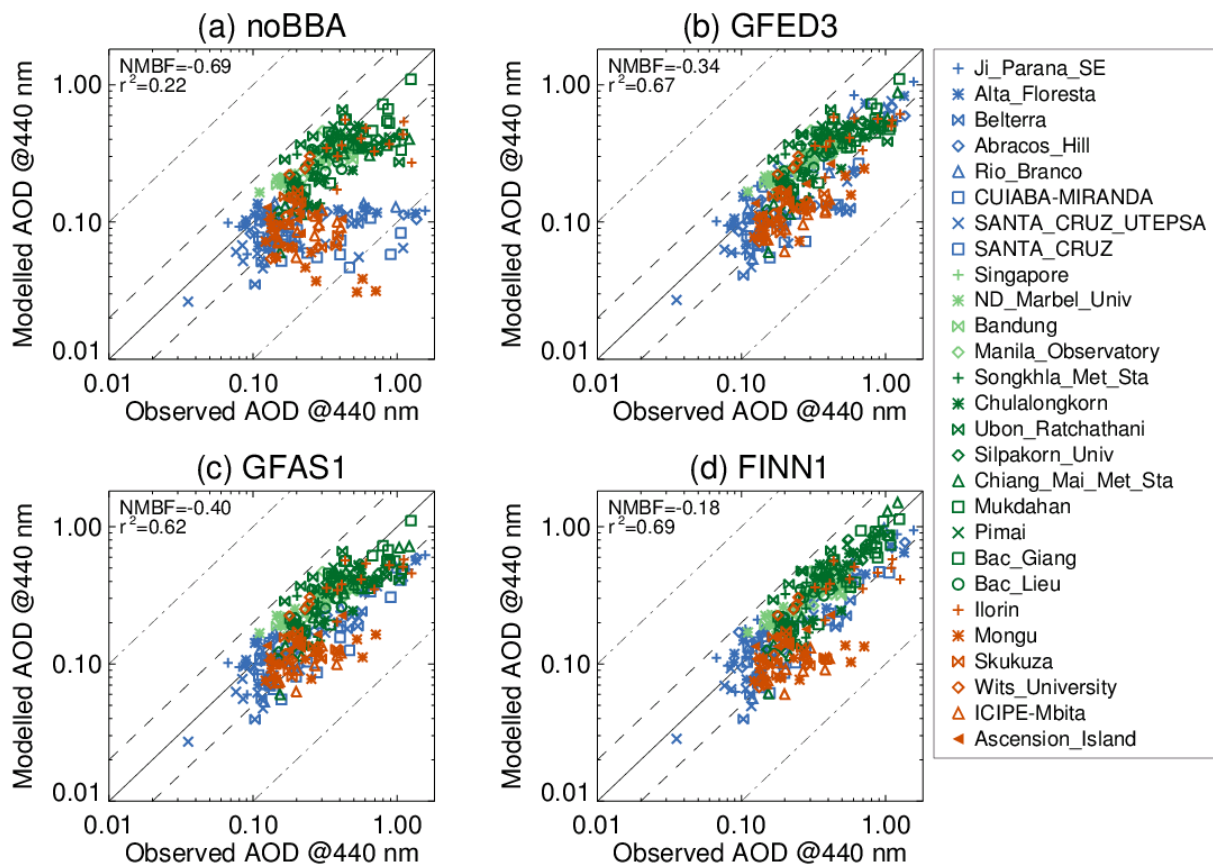


1
 2 **Figure 4.** Average seasonal cycles in observed (black) and simulated (colour) multi-annual monthly
 3 mean PM_{2.5} concentrations at four ground stations in the Amazon region: **(a)** Porto Velho (2009-
 4 2011); **(b)** Manaus (2008-2011); **(c)** Santarem (2003-2006); and **(d)** Alta Floresta (2003-2004). Multi-
 5 annual monthly mean concentrations were calculated by averaging over all years of available
 6 observation data between January 2003 and December 2011. The modelled results are shown for four
 7 simulations: without biomass burning (purple), with GFED3 emissions (red), with GFAS1 emissions
 8 (blue) and with FINN1 emissions (green). The error bars show the standard deviation of the mean of
 9 the observed and simulated values, which represents the inter-annual and intra-monthly variability in
 10 the daily mean PM_{2.5} concentrations.

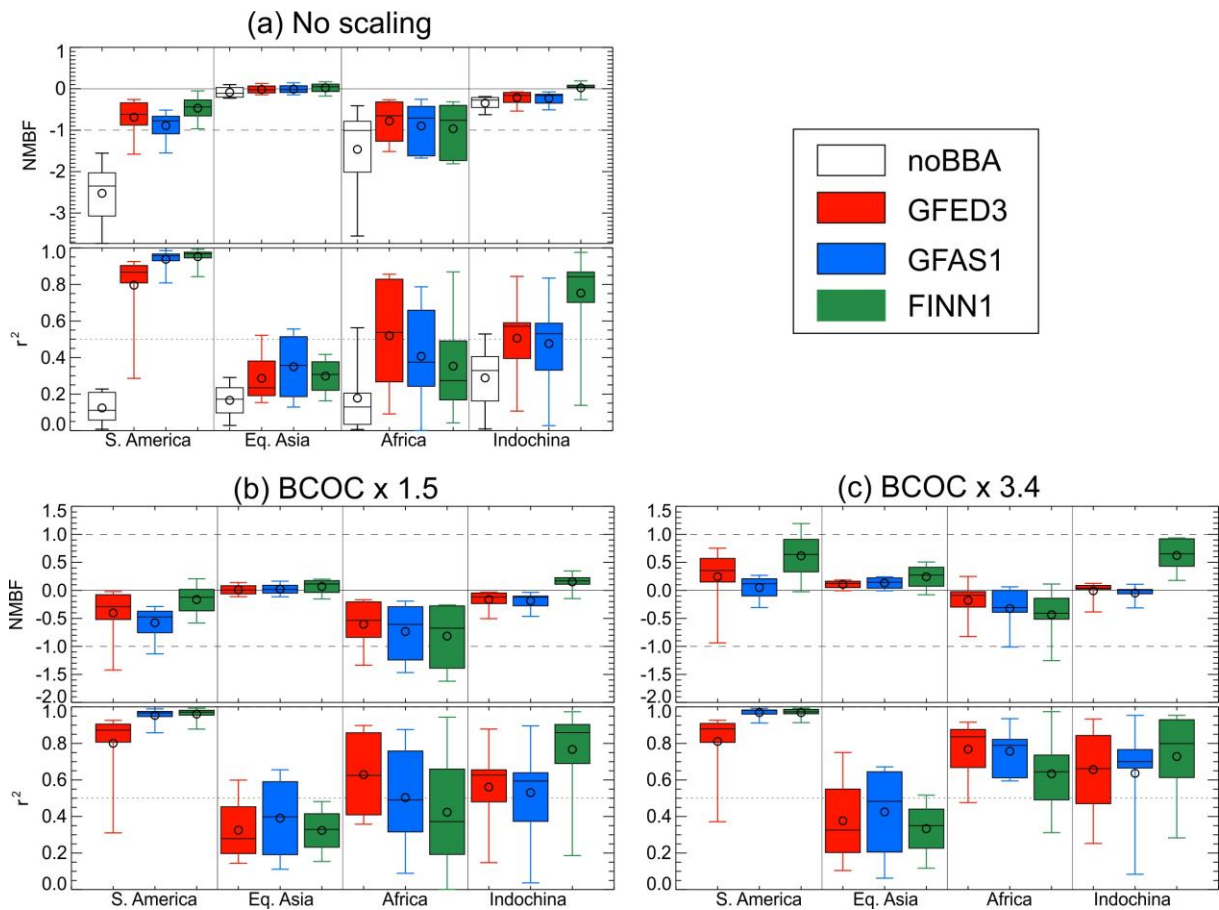
11

12

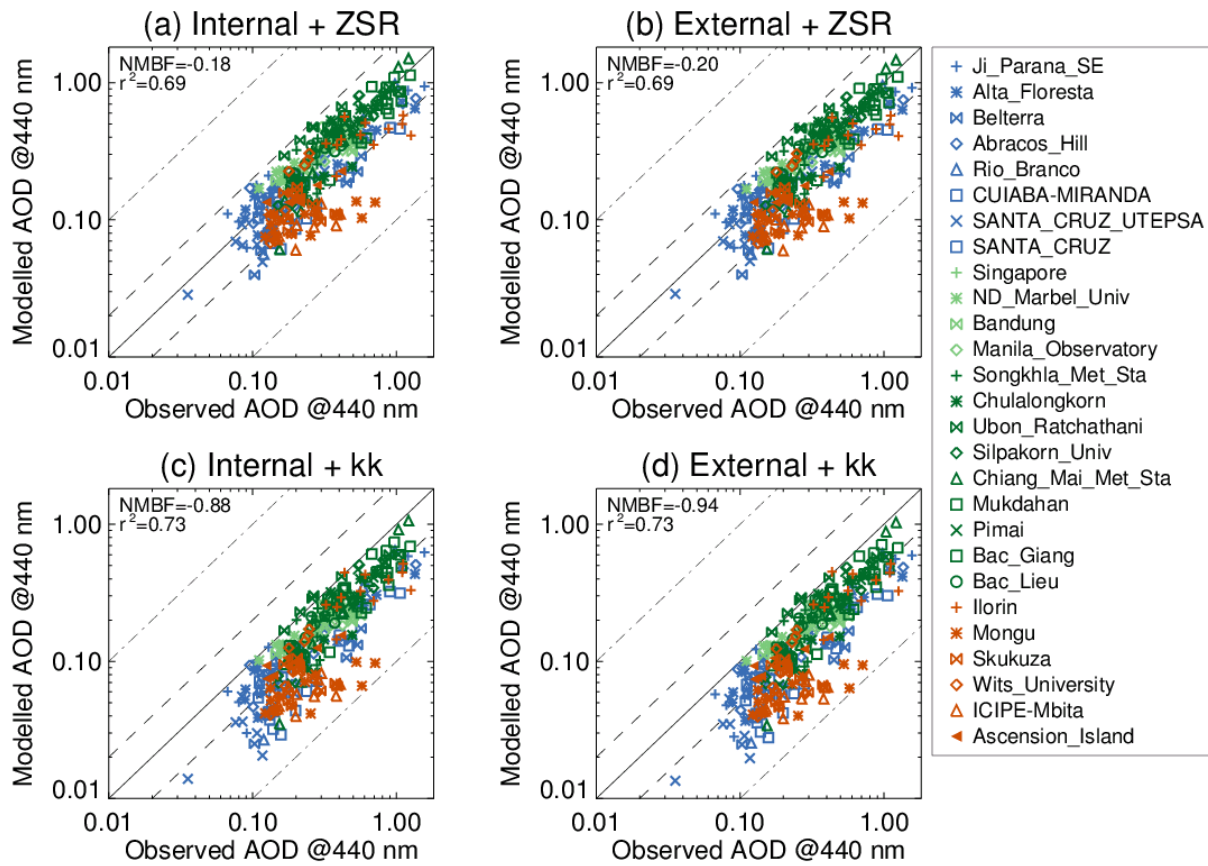
13



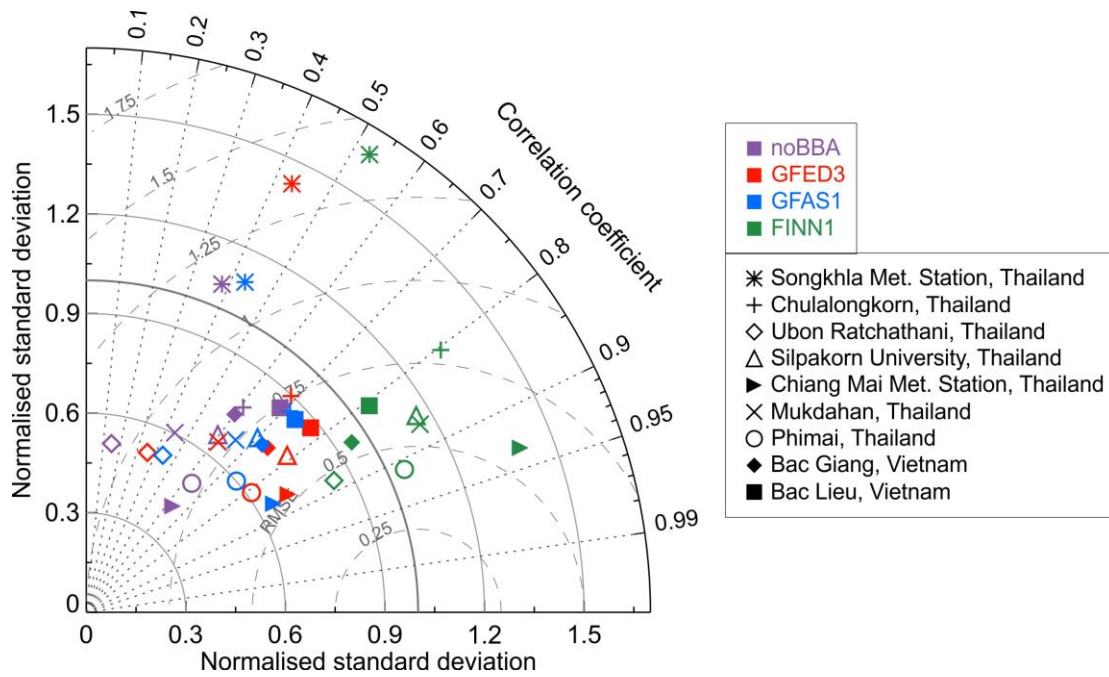
1
2 **Figure 5.** Simulated versus observed multi-annual monthly mean AOD at 440 nm at each AERONET
3 station. The model is shown (a) without biomass burning emissions, and with (b) GFED3, (c) GFAS1
4 and (d) FINN1 emissions. As for Fig. 2, the multi-annual monthly mean AODs were calculated using
5 all years of daily mean data available between January 2003 and December 2011 to obtain an average
6 seasonal cycle at each station. AERONET stations located in South America are shown in blue;
7 stations in Southeast Asia are shown in green (stations in Equatorial Asia and Indochina in light and
8 dark green, respectively); and stations in Africa are shown in orange. The normalised mean bias factor
9 (NMBF) and Pearson's correlation (r^2) between modelled and observed PM_{2.5} concentrations are
10 shown in the top left corner.
11



1
2 **Figure 6.** Box and whisker plots of the normalised mean bias factor (NMBF) and Pearson's
3 correlation coefficient (r^2) between modelled and observed multi-annual monthly-mean AOD at 440
4 nm for AERONET stations located in South America (8 sites), Equatorial Asia (4 sites), Africa (6
5 sites) and Indochina (9 sites). Results are shown for four model simulations: without fires (white), and
6 with each of the three biomass burning emissions inventories: GFED3 (red), GFAS1 (blue), FINN1
7 (green). (a) No scaling applied to the fire emissions; (b) particulate (BC/OC) fire emissions scaled up
8 globally by a factor 1.5; (c) particulate (BC/OC) fire emissions scaled up globally by a factor of 3.4.
9 The dashed lines indicate NMBFs of -1 and 1, which equate to an underestimation and overestimation,
10 respectively, of a factor of 2. The dotted line indicates an r^2 value of 0.5.

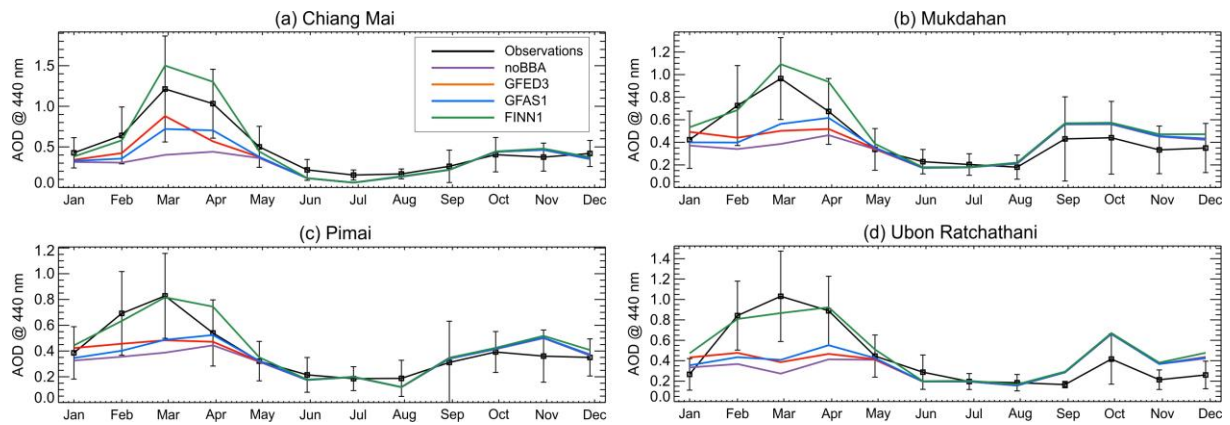


1
2 **Figure 7.** Simulated versus observed multi-annual monthly mean AOD at 440 nm at each AERONET
3 station to demonstrate the sensitivity of simulated AOD to different assumptions. The model is with
4 FINN1 fire emissions and simulated AOD is calculated assuming (a) internal mixing with ZSR water
5 uptake scheme (identical to Fig. 5d), (b) external mixing with ZSR water uptake scheme, (c) internal
6 mixing with κ -Köhler water uptake scheme, and (d) external mixing with κ -Köhler water uptake
7 scheme. AERONET stations located in South America are shown in blue; stations in Southeast Asia
8 are shown in green (stations in Equatorial Asia and Indochina in light and dark green, respectively);
9 and stations in Africa are shown in orange. The normalised mean bias factor (NMBF) and Pearson's
10 correlation (r^2) between modelled and observed PM_{2.5} concentrations are shown in the top left corner.
11



1
 2 **Figure 8.** Taylor diagrams (Taylor, 2001) comparing monthly mean modelled and observed AOD
 3 (440 nm) at 9 AERONET stations located in Indochina. The modelled and observed monthly mean
 4 AODs were calculated for every month with available daily mean data between January 2003 and
 5 December 2011. The observations are represented by a point on the x-axis at unit distance from the y-
 6 axis. The results are shown for four simulations: without biomass burning (purple), and with GFED3
 7 (red), GFAS1 (blue) and FINN1 (green) fire emissions. The model standard deviation and root mean
 8 square error (RMSE) are normalised by dividing by the corresponding observed standard deviation.
 9 The normalised standard deviation and RMSE values are marked by the grey-solid and grey-dashed
 10 lines respectively. The correlation coefficient (r) values are marked by the grey dotted lines.

11
 12
 13
 14
 15
 16



1
 2 **Figure 9.** Average seasonal cycles in observed (black) and simulated (colour) monthly mean AOD at
 3 440 nm at four AERONET stations in the Thailand: **(a)** Chiang Mai Met. Station; **(b)** Mukdahan; **(c)**
 4 Phimai; and **(d)** Ubon Ratchathani. Multi-annual monthly mean concentrations were calculated by
 5 averaging over all years of available daily mean observation data between January 2003 and
 6 December 2011. The modelled results are shown for four simulations: without biomass burning
 7 (purple), and with GFED3 (red), GFAS1 (blue) and FINN1 (green) fire emissions. The error bars show
 8 the standard deviation of the mean of the observations.

9